Towards a Robust Hydrologic Data Assimilation System for Hurricane-induced River Flow Forecasting

[1]Peyman Abbaszadeh, [1]Fatemeh Gholizadeh, [2]Keyhan Gavahi, [2]Hamid Moradkhani

[1]Department of Civil and Environmental Engineering, Hydrologic Modeling and Assimilation Lab, Portland State University, Portland, OR, USA

[2]Center for Complex Hydrosystems Research, Department of Civil, Construction and Environmental Engineering, The University of Alabama, AL, USA

Correspondence to: Peyman Abbaszadeh (pabbaszadeh@pdx.edu)

Abstract

The Hybrid Ensemble and Variational Data Assimilation framework for Environmental Systems (HEAVEN) is a method developed to enhance hydrologic model predictions while accounting for different sources of uncertainties involved in various layers of model simulations. While the effectiveness of this data assimilation in forecasting streamflow have been proven in previous studies, its potential to improve flood forecasting during extreme events remains unexplored. This study aims to demonstrate this potential by employing HEAVEN to assimilate streamflow data from United States Geological Survey (USGS) stations into a conceptual hydrologic model to enhance its capability to forecast hurricane-induced floods across multiple locations within three watersheds in the Southeastern United States. The SAC-SMA hydrologic model is driven by two variables: precipitation and Potential Evapotranspiration (PET), collected from phase 2 of the North American Land Data Assimilation System (NLDAS-2) and MODIS (Moderate Resolution Imaging Spectroradiometer) satellite data, respectively. We have validated the probabilistic streamflow predictions during five instances of hurricane-induced flooding across three regions. The results show that this data assimilation approach significantly improves hydrologic model's ability to forecast extreme river flows. By accounting for different sources of uncertainty in model predictions—in particular model structural uncertainty in addition to model parameter uncertainty, and atmospheric forcing data uncertainty, the HEAVEN emerges as a powerful tool for enhancing flood prediction accuracy. The study found that data assimilation improved streamflow forecasting during Hurricane Harvey, enhancing the SAC-SMA model's accuracy across most USGS stations on the peak flow day. However, data assimilation had little effect on streamflow forecasting for Hurricane Rita. In Rita, the streamflow surged dramatically in a single day (from 28 m^3/s to 566 m^3/s), causing the model to miss the high flow event despite accurate initialization the day before. For Hurricanes Ivan and Matthew, data assimilation

improved peak flow forecasts by 21% to 46% in Mobile and 5% to 46% in Savannah, with improvements varying by station location.

Keywords: Data Assimilation; Hydrologic Modeling; Extreme Event; Hazard; Uncertainty Quantification

1. Introduction

Floods rank among the most devastating and destructive natural calamities globally, annually causing significant economic losses and fatalities. According to the United Nations report, flooding alone affected 2.3 billion people globally from 1995 to 2015 (Wahlstrom and Guha-Sapir, 2015). The literature indicates that climate change will amplify the magnitude and frequency of river flooding across the United States (Mallakpour and Villarini, 2015; Alipour et al., 2020b). This is due to the warming climate that leads to more evaporation from land and ocean, which in turn increase the size and frequency of the heavy precipitation events, and therefore, escalate the flooding risk (Alipour et al., 2020a; Blöschl et al., 2019).

A flood modeling system is indispensable to increase the resiliency of communities prone to flooding by minimizing and mitigating their consequences and impacts. Developing an accurate and reliable flood forecasting and inundation system requires multiple components, including: 1) a numerical weather prediction model to estimate the atmospheric forcing variables such as precipitation, 2) a hydrological model to simulate the rainfall-runoff process and other hydrologic fluxes such as streamflow, and 3) a hydrodynamic model for streamflow routing and flood inundation mapping (Grimaldi et al., 2019; Jafarzadegan et al., 2023). Hydrologic and hydrodynamic models together constitute a pivotal part of the flood inundation mapping task, which enables the decision-makers to execute safe urban planning and operational risk management (Annis et al., 2020; Zischg et al., 2018). Existing literature reveals numerous studies

concentrating on rainfall-runoff processes and floodplain dynamics, as well as the development of integrated hydrologic and hydrodynamic models. These efforts aim to enhance flood forecasting, assess flood risks, and model flood hazards across spatio-temporal scales (e.g., Felder et al., 2017; Laganier et al., 2014; Mai and De Smedt, 2017; Nguyen et al., 2016; Sindhu and Durga Rao, 2017; Tripathy et al., 2024).

Flood predictions and inundation maps are often inaccurate and erroneous due to different sources of uncertainties involved in different layers of the modeling chain (Ahmadisharaf et al., 2018; Annis et al., 2020; Apel et al., 2004). These include the hydraulic model structure, parameters (e.g., channel and floodplain roughness values), and boundary conditions, that is the upstream and downstream river discharge. While many studies underscore the significance of addressing uncertainties associated with channel and floodplain friction parameters (Aronica et al., 2002; Bates et al., 2004; Papaioannou et al., 2017; Pappenberger et al., 2005; Werner et al., 2005), channel geometry (Bhuyian et al., 2015; Neal et al., 2015), model structure (Dimitriadis et al., 2016; Liu et al., 2019; Petroselli et al., 2019), and input Digital Elevation Model (DEM) resolution (Petroselli et al., 2019) in assessing the uncertainty of inundation mapping, little attention has been given to uncertainties within the hydrologic processes directly impacting flood modeling performance. In most of these studies, the hydrological uncertainties are related to the rating curves (Bermúdez et al., 2017; Di Baldassarre and Montanari, 2009; Domeneghetti et al., 2012; Pappenberger et al., 2006) and the shape of the flow hydrographs (Domeneghetti et al., 2013; Scharffenberg and Kavvas, 2011; Savage et al., 2016), but they did not explicitly account for the uncertainty associated with different components of the hydrologic model predictions, such as the forcing data uncertainty (due to the limitation of measurements and spatiotemporal representativeness of the data), model parameter uncertainty (due to conceptualization of the

model and non-uniqueness of parameters), model structural uncertainty due to the imperfect representation of a real system (Pathiraja et al., 2018; Parrish et al., 2012), and initial and boundary condition uncertainty (Abbaszadeh et al., 2018a; Moradkhani et al., 2018a). This study seeks to account for all the aforementioned sources of uncertainties involved in hydrologic model predictions within a Bayesian framework and studies their impacts on hurricane-induced extreme river discharges across different regions in the Southeastern United States (SEUS). It is expected that reducing hydrologic uncertainties result in improving the accuracy and reliability of flood inundation mapping when the enhanced hydrologic forecasts are utilized to drive the hydrodynamic model.

Bayesian methods have been extensively utilized in a numerous studies to characterize, quantify and reduce the uncertainties in hydrologic model predictions (Abbaszadeh et al., 2020; Dechant and Moradkhani, 2012; Kuczera and Parent, 1998; Marshall et al., 2004; Moradkhani et al., 2005; Pathiraja et al., 2018b; Yan and Moradkhani, 2016). Data Assimilation (DA) is a well-received Bayesian approach in the hydrometeorological community to account for the uncertainties involved in different components of hydrologic model predictions by probabilistically conditioning the states of the model on observations (Moradkhani et al., 2005; Liu and Gupta 2007; Clark et al. 2008; Vrugt et al. 2006; Moradkhani et al. 2018; Abbaszadeh et al. 2018). The DA methods based on the Ensemble Kalman Filter (EnKF) and Particle Filter (PF) are commonly used to recursively estimate both states and parameters. In these methods, Monte Carlo sampling and sequential updating are applied to not only a vector of model parameters but also to a set of prognostic and diagnostic state variables at each assimilation step (see Moradkhani et al., (2018) and references therein). The probability distributions of both model states and parameters are recursively and independently updated at each time step as new observations

become available. These approaches yield more accurate state and parameter estimates compared to open-loop simulation (without data assimilation), allowing the modeling system to evolve consistently over time. As a result, this leads to improved model predictions while accounting for uncertainties. (Yan et al. 2015; Plaza et al. 2012; Hain et al. 2012; Lee et al. 2011; Lievens et al. 2016; Dechant and Moradkhani 2012, 2011; Abbaszadeh et al. 2018; Montzka et al. 2013; Koster et al. 2018).

In this study, we utilize a recently developed state-of-the-art hydrologic data assimilation method, hereafter referred to as Hybrid Ensemble and Variational Data Assimilation framework for Environmental Systems (HEAVEN), to address all sources of uncertainties (i.e., forcing data, parameters, model structure, and initial conditions) in hydrologic simulations (Abbszadeh et al., 2019). In particular, we study its usefulness and effectiveness in enhancing peak flow forecasts during an extreme event. Although the capability of this method, in conjunction with hydrological models for streamflow forecasting, has been demonstrated in previous studies, its ability to capture peak flows induced by heavy rainfall from hurricanes—common in southeastern regions—has not been explored. This study aims to address this gap and contribute to enhancing the resiliency of the SEUS, a region particularly vulnerable to extreme flooding due to hurricanes and tropical cyclones. By improving streamflow forecasting during such events, the study seeks to better inform flood management strategies and mitigate the impacts of future extreme weather events in these high-risk areas. The remainder of the paper is organized as follows. In Section 2, we present the materials and methods, encompassing the study areas and datasets, descriptions of the hydrologic model, data assimilation, and calibration methods. Section 3 examines the results of the hydrologic data assimilation and its advantages in enhancing peak flow forecasts. Section 4 outlines the conclusions and provides suggestions for further expanding this research in the future.

2. Materials and Methods

This section first describes study areas and datasets used in this study, then introduces the hydrologic model that is used for streamflow prediction, and provides a summary for the model calibration and data assimilation methods.

2.1 Study Areas

This study is conducted over three watersheds in three different states in the southeast US. Figure 1 illustrates their geographical locations along with all the available United States Geological Survey (USGS) stations within those regions. Galveston, Mobile, and Savanah are the three watersheds located in hurricane-prone regions near the coast in the state of Texas, Alabama, and Georgia, respectively. These three watersheds encompass Galveston Bay, Mobile Bay, and Savanah Bay, respectively.

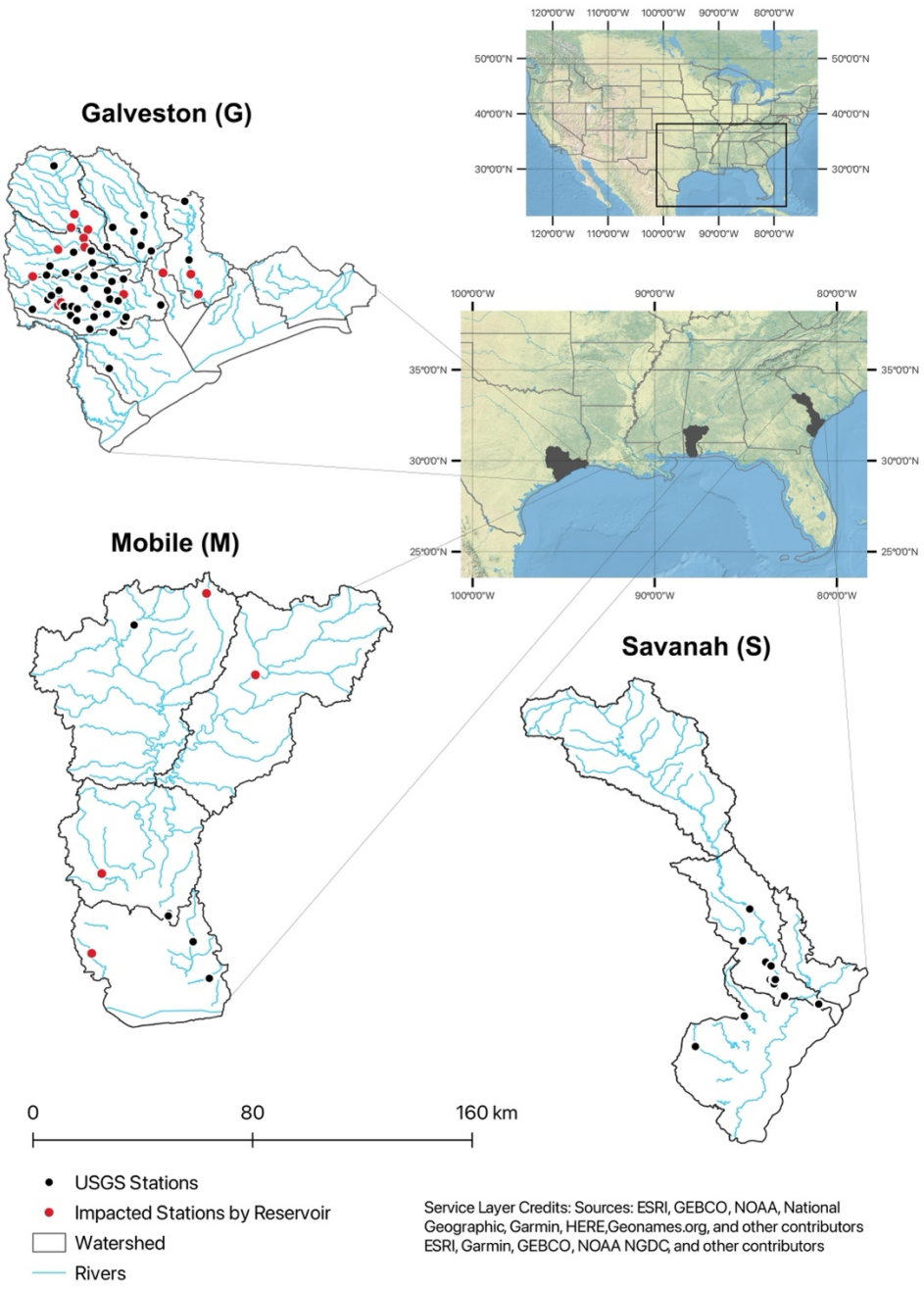

Figure 1. Location of Galveston, Mobile, and Savanah watersheds in three different states in the southeast US. Black points represent the USGS stations operated in each watershed.

To provide a comprehensive analysis and show the robustness of the proposed approach in accounting for the uncertainties involved in hydrologic predictions and its benefit in generating accurate and reliable flood inundated areas, we conducted this study over five hurricane-induced

161 flooding events in three different regions in the SEUS. These include hurricane Harvey and Rita
162 (in Galveston watershed), Hurricane Ivan (in Mobile watershed), and Hurricane Matthew and Irma
163 (in Savanah watershed). The Galveston watershed comprises nine HUC8s, including 12040202
164 (East Galveston Bay), 12040203 (North Galveston Bay), 12040102 (Spring), 12040103 (East Fork
165 San Jacinto), 12040201 (Sabine Lake), 12040204 (West Galveston Bay), 12040205 (Austin-
166 Oyster), 12040101 (West Fork San Jacinto), and 12040104 (Buffalo-San Jacinto). The climate in
167 this region is humid subtropical with prevailing winds from the south and southeast that bring heat
168 from the deserts of Mexico and moisture from the Gulf of Mexico. This watershed has a long, hot,
169 and humid summer, such that the temperature exceeds above 32 °C in August, while the winter is
170 often mild and the temperature does not usually drop below 4 °C. Snowfall in Galveston is
171 generally rare, while the rainfall is frequent. With an average of 1000 mm, the rainfall is higher
172 than the national average (767 mm). Hurricanes and tropical storms are notorious for wreaking
173 havoc on the region's economy and environment and putting several communities at risk,
174 including Houston, which is the fifth-largest metropolitan region in the US. In August 2017,
175 hurricane Harvey with heavy rainfall and wind storms hit the Galveston area and caused significant
176 flooding. Many locations around the bay area (i.e., Harris and Galveston counties) experienced
177 more than 760 mm of rain in a few days that resulted in $23 billion in property damages, according
178 to Reuters report (McNeill and Wilson, 2017). In September 2005, hurricane Rita swept through
179 east Texas and the Louisiana coast and resulted in extensive flooding, damages, and more than a
180 hundred fatalities. Rita is the most intense tropical cyclone in the history of the Gulf of Mexico.
181 According to the National Oceanic and Atmospheric Administration (NOAA) report (Knabb and
182 Brown, 2006), Rita’s wind storm resulted in some flooding across the river networks in northern
183 regions of the Galveston Bay by pushing the river water southward.

184 The Mobile watershed only refers to the lower portion of the Mobile basin which consists
185 of four HUC8s, including 03150204 (lower Alabama), 03160204 (Mobile-Tensaw), 03160205
186 (Mobile Bay), and 03160203 (Lower Tombigbee). This region is characterized by a warm and
187 temperate climate with well distributed high rainfall throughout the year. Even in the driest month
188 of the year, this area experiences significant rainfall. The precipitation usually is in the form of
189 rain, such that on average the annual rainfall reaches 1600 mm - almost two times more than the
190 US average rainfall per year. In this watershed, summer is long and hot, and the winter is short and
191 cold. In the warmest and coldest months of the year, the temperature usually does not rise above
192 32 °C and does not fall below 5 °C. In September 2004. Hurricane Ivan made landfall along the
193 coasts from Destin in the Florida panhandle westward to Mobile Bay/Baldwin County, Alabama,
194 according to the NOAA report (NOAA, 2005). The rainfall of this hurricane caused major flooding
195 in both Alabama and northwest Florida. According to the National Weather Services
196 (https://www.weather.gov/mob/ivan), Ivan resulted in nearly $14 billion in damage in both states.
197 The radar-estimated data shows the rainfall associated with hurricane Ivan over the coastline of
198 Alabama (near Orange Beach) reached more than 381 mm and then gradually decreased as the
199 hurricane's eye moved northward.
200 The third watershed used in this study is Savanah, which is comprised of four HUC8s,
201 including 03060106 (Middle Savannah), 03060109 (Lower Savannah), 03060110 (Calibogue
202 Sound-Wright River), and 03060204 (Ogeechee Coastal). This watershed has a humid subtropical
203 climate with long hot summers and temperate winters. In this region, the precipitation is mainly
204 influenced by the Atlantic Ocean (from the east side) and the Appalachian Mountains (from the
205 west side). The precipitation is usually in the form of rainfall throughout the year with some rare
206 snowstorms that occur in the northern mountainous regions in winter. Climate change has a serious

207 impact in Savanah because of the severe heat and intense storms that cause periods of drought and
208 flood, putting the region's water and food supplies at risk (Ingram, 2013; Knox and Mogil 2020).
209 The temperature usually does not go below 4 °C and over 34 °C in the coldest and warmest months
210 of the year. November and August are the driest and wettest months of the year with an average
211 precipitation of 61 mm and 183 mm, respectively. As shown in Figure 1, the predominant land
212 cover in Savanah is wetlands. In October 2016, Hurricane Matthew with strong winds and heavy
213 rainfall hit the coastline of South Carolina and North Carolina and caused extensive coastal and
214 inland flooding. The National Hurricane Center (NHC) reported dozens of deaths and $10 billion
215 in damages across the US East Coast (Stewart, 2017). According to the NOAA report, Hurricane
216 Matthew produced a copious amount of rain that led to record-breaking river levels in some
217 locations in the Savannah region (Liberto, 2016). A year after that, in September 2017, this region
218 was again hit by Category 5 Hurricane Irma. The hurricane's wind speed exceeded 60 mph in the
219 Savanah region that resulted in a significant tidal surge in the Savanah River, according to the
220 National Weather Service. The storm surge and tide together produced maximum inundation levels
221 of 3 to 5 ft above ground level along the coast of Georgia and much of South Carolina that inflicted
222 extensive damages to infrastructure, agriculture, and properties (Cangialosi and Latto, 2017).

223 **2.2 Datasets**

224 We used Moderate Resolution Imaging Spectroradiometer (MODIS) Potential
225 Evapotranspiration (PET), and Phase 2 of the North American Land Data Assimilation System
226 (NLDAS-2) precipitation forcing data to drive the hydrologic model and estimate the streamflow.
227 The streamflow observations collected from the USGS stations were used for calibration,
228 assimilation, and validation purposes. To collect the USGS streamflow data, we used *Climata*
229 (https://github.com/heigeo/climata) which is a python package that facilitates acquiring climate

and water flow data from a variety of organizations such as NOAA, National Weather Service (NWS), and USGS. The documentation of this package along with example scripts are available at Earth Data Science (2021).

2.2.1 MODIS

MODIS global evapotranspiration product MOD16 is a gridded land surface ET data set for the global land areas at 8-day, monthly and annual intervals (Mu et al., 2011, 2007). The output variables of the MOD16 product include 8-day, monthly and annual ET, λE (latent heat flux), potential ET (PET), PλE (potential λE), and ET_QC (quality control). In this study, we used MOD16A2 PET product at 500 m spatial resolution and 8-day time-interval. Please note that the pixel values for PET are the sum of all eight days within the composite period. The dataset can be retrieved from https://lpdaac.usgs.gov/products/mod16a2v006/.

2.2.2 NLDAS-2

NLDAS-2 contains quality-controlled, and spatially and temporally consistent meteorological forcing data, such as surface downward shortwave radiation, surface downward longwave radiation, specific humidity, air temperature, surface pressure, near-surface wind in u and v components, and precipitation rate. In this study, we used precipitation data from the NLDAS_FORA0125_H product, which has been widely used to derive hydrology and land surface models. This dataset is available from 1979 to present with a spatial resolution of 1/8° and temporal resolution of 1 hour (Xia et al., 2012). This data can be retrieved from https://disc.gsfc.nasa.gov/datasets/NLDAS_FORA0125_H_002/summary.

2.3 SAC-SMA Hydrologic Model

In this study, we used Sacramento Soil Moisture Accounting Model (SAC-SMA) to simulate the streamflow at several locations within three different watersheds. The SAC-SMA

253 (Burnash et al., 1973) is a lumped-parameter model that represents each basin vertically by two
254 soil zones: an upper zone and a lower zone (Gourley et al., 2014). The upper and lower zones
255 represent the short-term storage capacity and long-term groundwater storage, respectively. For
256 descriptions of model parameters and state variables, we refer the readers to our previous study
257 (Burnash et al., 1973; Abbaszadeh et al., 2018). This model is widely used by the NOAA/NWS
258 for operational flood forecasting in the US (Smith et al., 2003; Lee et al., 2016; Kratzert et al.,
259 2018; Gourley et al., 2014). SAC-SMA produces daily streamflow from daily PET and
260 precipitation data. It is noted that here we disaggregated and aggregated the MODIS PET and
261 NLDAS precipitation data, respectively, to 6-hour interval in order to be consistent with the SAC-
262 SMA hydrologic model that generally runs at a 6-hour time step. SAC-SMA model inputs include
263 6-hour Mean Areal Precipitation (MAP) and 6-hour Mean Areal Potential Evapotranspiration
264 (MAPE). These variables are calculated by delineating the drainage area contributing to each
265 USGS station for which the hydrologic model is performed.

266 In this study, we employ the SAC-SMA model to simulate flooding events triggered by
267 hurricanes occurring post-2001, as the MODIS-derived PET data necessary to drive the hydrologic
268 model is available starting from 2001. Recent studies (Bennett et al., 2019; Bowman et al., 2017)
269 showed that using MODIS PET as input to the SAC-SMA model results in more reliable
270 streamflow simulations compared to traditional evapotranspiration (ET) demand.

271 **2.4 Data Assimilation**

272 In this study, we use Hybrid Ensemble and Variational Data Assimilation framework for
273 Environmental Systems, HEAVEN (Abbaszadeh et al., 2019) to account for all sources of
274 uncertainties involved in the hydrologic model simulations. HEAVEN is a data assimilation
275 method built through the combination of a deterministic four-dimensional variational (4DVAR)

assimilation method with the PF ensemble data assimilation system. Since we already provided a comprehensive description of this data assimilation approach in Abbaszadeh et al. (2019), here we briefly describe its formulation and implementation process. HEAVEN provides the possibility that both sequential and variational assimilation approaches can effectively feed each other in a single framework to produce a more complete representation of posterior distributions. The first step is to minimize the weak-constraint 4DVAR cost function (Eq. 1) within an assimilation cycle and find the optimal initial condition, which is also known as analysis $\mathrm{x_a}$. For the time period of T and assimilation window size K ($[t_0, t_{k=K}]$), the number of assimilation cycles in the HEAVEN becomes T/K. For example, for a one year analysis period of $T = 365$ days, with the assumption of $K = 5$ days, 73 assimilation cycles or windows are defined. In each assimilation cycle, k ranges between 0 to K, where $k = 0$ indicates the initial time step. The optimal solution is the joint maximum likelihood estimate of the state variables within the assimilation window given the observations. The only free variable in the minimization of the cost J is the model state x_0 at the initial time t_0. The optimal solution (analysis) is obtained through an iterative method that, typically, relies on linearized versions of the model and observational operator to obtain a quadratic approximation to the cost J (outer iteration) and adjoint modeling for gradient information.

$$\mathrm{J(x_0, \dots, x_K) = J^b + J^o + J^q}$$

$$= \frac{1}{2}\left(\mathrm{x_0 - x_{0,b}}\right)^{\mathrm{T}} \mathrm{B^{-1}} \left(\mathrm{x_0 - x_{0,b}}\right) + \frac{1}{2}\sum_{\mathrm{k=0}}^{\mathrm{K}} \left(\mathrm{y_k - h_k(x_k)}\right)^{\mathrm{T}} \mathrm{R_k^{-1}} \left(\mathrm{y_k - h_k(x_k)}\right)$$

$$+ \frac{1}{2}\sum_{\mathrm{k=1}}^{\mathrm{K}} \left(\mathrm{x_k - \mathcal{M}_{k-1\rightarrow k}(x_{k-1}, \Theta, u_k)}\right)^{\mathrm{T}} \mathrm{Q^{-1}} \left(\mathrm{x_k - \mathcal{M}_{k-1\rightarrow k}(x_{k-1}, \Theta, u_k)}\right) \qquad (1)$$

k and K show time step in each assimilation window and assimilation window size, respectively. B, $\mathrm{R_k}$, $\mathrm{Q_k}$ specify prior, observation, and model error covariance matrices respectively. Initial deterministic guess for state variables and parameters are also respectively represented by $\mathrm{x_{0,b}}$ and

Θ. h and $\mathcal{M}$ represent the observation and model operators. y_k and u_k are the observation and forcing data at time step k. To initialize the system, the error covariance matrices are calculated as follows:

$$R_k = (\max((\lambda \times y_k), 1))^2 \qquad (2)$$

$$B = \mathrm{diag}\left((\Omega \times x_{0,b})^2\right) \qquad (3)$$

$$Q_k = \Gamma \times \mathrm{diag}\left((\pi \times x_{0,b})^2\right) \qquad (4)$$

where λ is the error percentage in observations. Ω represents the error percentage in initial state variables $x_{0,b}$. π is the error percentage in model structure and Γ is the model error covariance inflation ($\Gamma \geq 1$) or deflation factor ($\Gamma \leq 1$). Since here the model covariance error is assumed to be static and does not vary in time, therefore in equation 1, Q_k becomes Q. The initial guess for the model parameters is obtained using the Latin Hypercube Sampling (LHS) approach. Since the minimum and maximum values of the model parameters are predefined (Abbaszadeh et al., 2018), the ensemble members of model parameters θ^i can be generated using the LHS. Here, the 4DVAR cost function is executed in a deterministic way, therefore it requires an ensemble mean of θ^i, which is calculated using the equation (5). N is the ensemble size.

$$\Theta = \frac{1}{N}\sum_{i=1}^{N} \theta^i \qquad (5)$$

The linearization of observation h and model $\mathcal{M}$ operations is required for performing variational data assimilation approaches. This hinders their use in hydrological applications because such linearizations are not usually feasible. To address this problem, we minimize the 4DVAR cost function and find the optimal solution x_a using the Nelder-Mead algorithm (Nelder and Mead, 1965), which is a derivative-free optimization method. 4DVAR seeks the initial condition such that the forecast best fits the observations within the assimilation interval. We

specify the model parameters Θ at each time step within the assimilation interval. We then find the best initial state variables (also known as analysis) x_a by minimizing the 4DVAR cost function.

Up to this point, the optimal initial condition $\mathrm{x_a}$ within the first assimilation window is obtained. To perform the particle filtering DA within the same assimilation window, we use $\mathrm{x_a}$ as an initial guess (prior information) with some error that follows a Gaussian distribution. In equation (6), $\mathrm{x_0^i}$ is the initial state ensemble members and B is the prior error covariance matrix used in the 4DVAR cost function.

$$\mathrm{x_0^i} = \mathrm{x_a} + \varepsilon^{\mathrm{i}} \qquad \varepsilon^{\mathrm{i}} \sim \mathrm{N}(0, \mathrm{B}) \qquad (6)$$

To ensure that an appropriate initial condition x_0^i is replicated for cycle τ, which later leads to better estimation of the posterior distributions in that window interval, we run the forward model for cycle τ using two initial ensemble scenarios: (1) x_0^i and (2) state posterior distribution obtained in the last time step ($k = K$) of assimilation cycle $\tau - 1$ (x_K^i). Under these two initial conditions, we calculate y_k^i for ensemble members within the assimilation interval $[t_0, t_K]$, and based on their discrepancies from the observations Obs_k, one can decide to preserve the particles x_0^i or replace them with those already available from the previous cycle $\tau - 1$.

Here, we refer readers to Appendix A, where we describe the implementation of the Evolutionary Particle Filter with Markov Chain (EPFM) data assimilation approach (Abbaszadeh et al., 2018). To facilitate the reproduction of HEAVEN, Figure 2 presents a schematic summarizing all the processes involved within this approach. Step 1 in this figure illustrates how the initial condition for the first window cycle is generated. As mentioned earlier, by minimizing the weak-constrained 4DVAR cost function, the optimal initial condition for the first cycle is obtained. Note that this is a deterministic value, which must be reshaped into an ensemble for

initialization of the sequential filtering process, as described in Step 2. In Step 3, the EPFM sequential filtering approach (explained in Appendix A) is used to calculate the posterior estimates of model states and parameters within the first assimilation cycle. Next, we use Eqs. A19 and A21 to calculate the dynamic error covariance matrix and the prior error covariance matrix. Finally, in Step 6, we use the updated error covariance matrix along with the expected values of the posterior estimates of model states and parameters to initialize the next assimilation cycle.

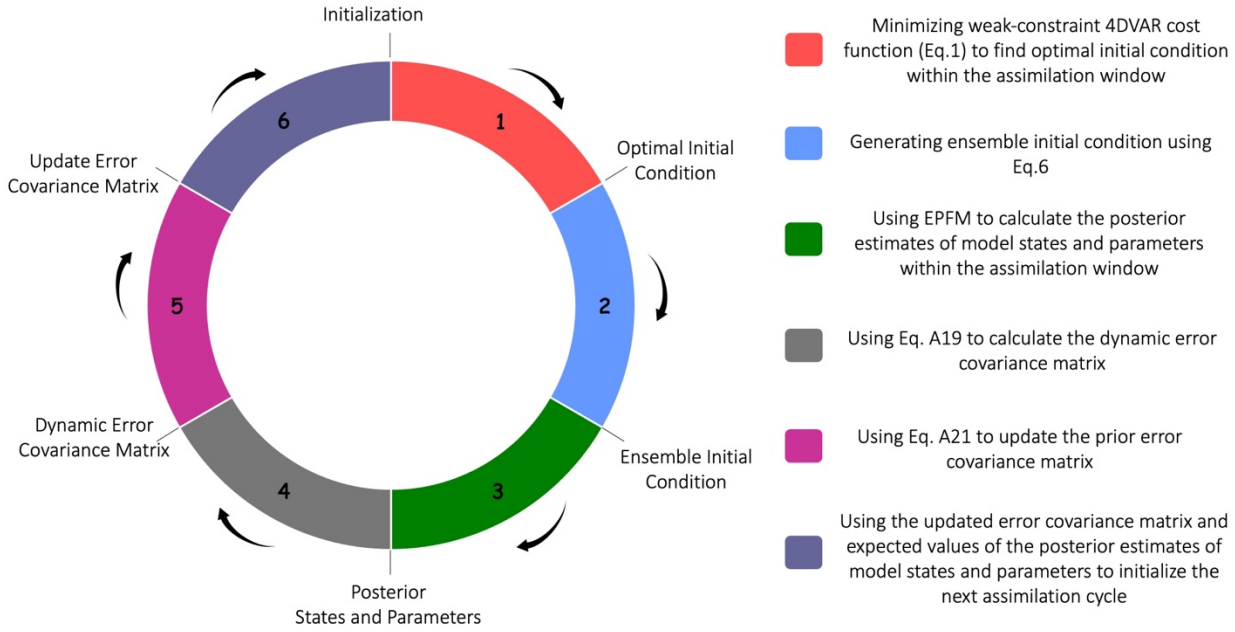

Figure 2: A schematic summarizing all the processes in HEAVEN.

The DA method utilizes the weak-constraint 4DVAR cost function (Eq. 1), which accounts for multiple sources of uncertainty by incorporating three key covariance matrices: B, R, and Q. These matrices represent different types of errors: B accounts for errors in the initial condition, R represents observational errors, and Q captures model structural errors. By explicitly modeling these errors, the method provides a more comprehensive and realistic representation of the uncertainty in the system. In addition to these sources of uncertainty, the method also considers the uncertainty associated with the forcing data. In the context of the EPFM approach, it is assumed

that errors exist in the forcing data, which can significantly affect model predictions. To account for this, we introduce white noise to the forcing variables, effectively perturbing the forcing data. This process generates an ensemble of forcing data, which is then used to drive the hydrological model. Thus, the DA method is designed to account for all major sources of uncertainty—initial condition errors, observational errors, model structural errors, and errors in the forcing data. By incorporating these uncertainties into the assimilation process, the method enhances the accuracy and reliability of the model predictions.

2.5 Model Calibration and Validation

Figure 3 illustrates the model calibration and validation periods used for all three watersheds. As depicted in the figure, the validation period was chosen to encompass the time frame of extreme flooding events in all study regions. This ensures the applicability of the calibrated model for predicting future events. To validate the calibrated model, we tested its ability to predict peak flow during a period that was not used for calibration. This helps assess the model's performance and generalizability to unseen data. For the hydrologic model calibration, we used the Shuffled Complex Evolution (SCE-UA) optimization technique introduced by Duan et al. (1992). In this study, we do not provide a detailed explanation of the SCE-UA method; instead, we refer the readers to the original articles for further information (Duan et al., 1992, 1993). We calibrated 14 parameters within the SAC-SMA model using 10-years historical USGS streamflow observations, consistent with the calibration period suggested by the NOAA/National Weather Service (Smith et al., 2003). The optimal parameter values at each USGS station were found by maximizing Nash Sutcliffe Efficiency (NSE) objective function that simultaneously considers mean, low, and high flows (Samuel et al., 2011).

The SAC-SMA model was calibrated separately for each drainage area associated with the USGS stations, rather than using the entire basin for the calibration process. This decision was based on the structure of the SAC-SMA model, which is a lumped model, meaning that it aggregates hydrological processes over a given area rather than considering them at individual sub-basins or locations. To ensure accurate representation of the hydrological processes, we calibrated and validated the model specifically at each USGS station, while carefully accounting for the drainage area contributing to each station's flow. This is important for accurately calculating the model's forcing input variables—such as mean areal precipitation and mean areal potential evapotranspiration—since these inputs depend on the spatial extent of the drainage area for each station. By focusing on the specific drainage area for each USGS station, we ensure that the model's inputs reflect the local conditions of the watershed, leading to more reliable and representative model calibration and validation results. This method also improves the model's ability to simulate hydrological processes at the station level while considering the variations in environmental factors across different parts of the basin.

To ensure reliable initial conditions for the model's state variables, a 3-month spin-up period was used at the beginning of both the calibration and validation periods. This warm-up period allowed the model to stabilize prior to the actual calibration and validation processes. The model state variables are those listed in Table 2 of our previous paper (Abbaszadeh et al., 2018).

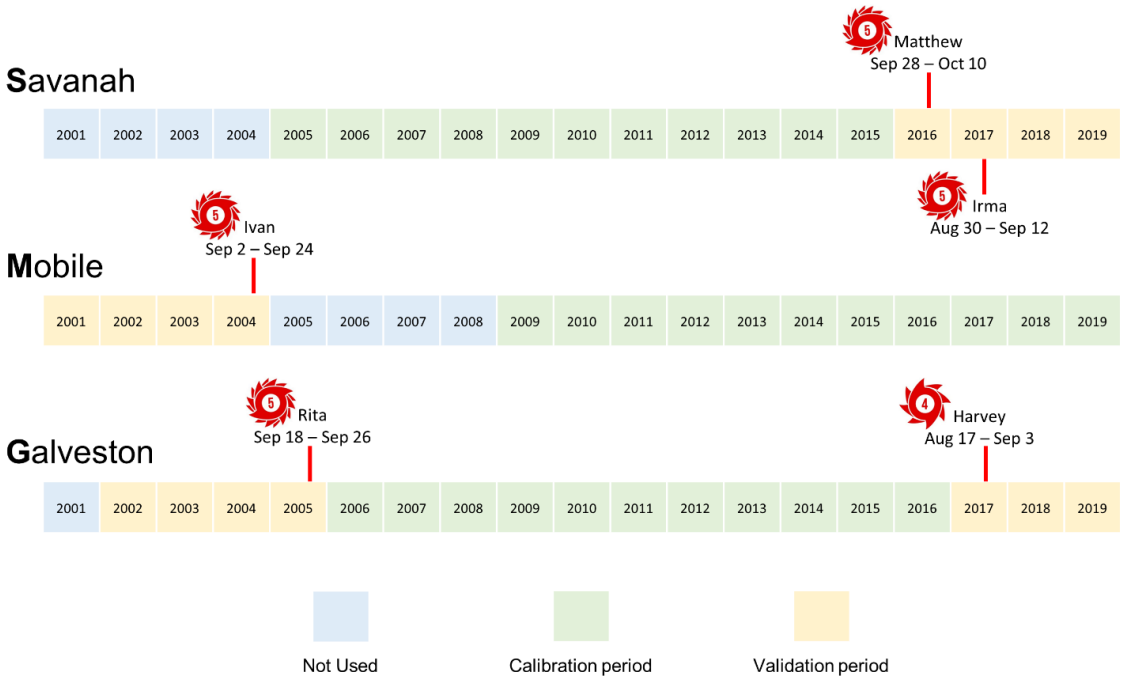

Figure 3. The calibration and validation periods considered in this study for three watersheds, along with the hurricane events and their respective durations.

3. Results and Discussions

This study aims to account for all sources of uncertainties involved in hydrologic model predictions and their impact on improving hurricane-induced extreme river discharges across different regions in the SEUS. This section summarizes the performance of the SAC-SMA hydrologic model during both the calibration and validation periods. It then explains the data assimilation settings along with the streamflow simulation capability of the SAC-SMA model with and without data assimilation. The study is conducted in multiple locations across three watersheds in the southeastern US during hurricane events**.**

3.1 SAC-SMA Model Calibration and Validation

Figure 4 illustrates the performance of the SAC-SMA model during both the calibration and validation periods across all study regions utilized in this research. As previously mentioned,

412 for parameter calibration of the SAC-SMA model, we utilized ten years of historical USGS
413 streamflow observation data, while model validation was conducted over a four-year period
414 encompassing flooding from various hurricane events (as shown in Figure 3). Within this figure,
415 the correlation coefficient (R), bias, and Root Mean Square Error (RMSE) represent the statistical
416 measures of the relationship between simulated and observed streamflow values. We remind that
417 in this study, we run the hydrologic model over those USGS locations that have not been affected
418 by the backwater effect of the downstream flow and the streamflow observations have always been
419 positive. These USGS locations are shown in Figure 1 with black dots. The results confirm that
420 although the SAC-SMA model was calibrated over the periods for which the river networks within
421 the watersheds have not experienced flow as much as the validation periods, the model parameters
422 were properly calibrated to simulate the streamflow. The model parameters are those listed in
423 Table 1 of our previous paper (Abbaszadeh et al., 2018). The temporal resolution of streamflow
424 simulation is daily. DA occurs at a daily time scale to match the output frequency of the SAC-
425 SMA model. This strategy aims to minimize the impact of instantaneous streamflow changes on
426 parameter updates during the assimilation process. While assimilating streamflow at sub-daily
427 intervals could be advantageous for adjusting model state variables such as soil moisture storage,
428 it is not anticipated to significantly contribute to updating model parameters, which typically vary
429 at coarser time scales.

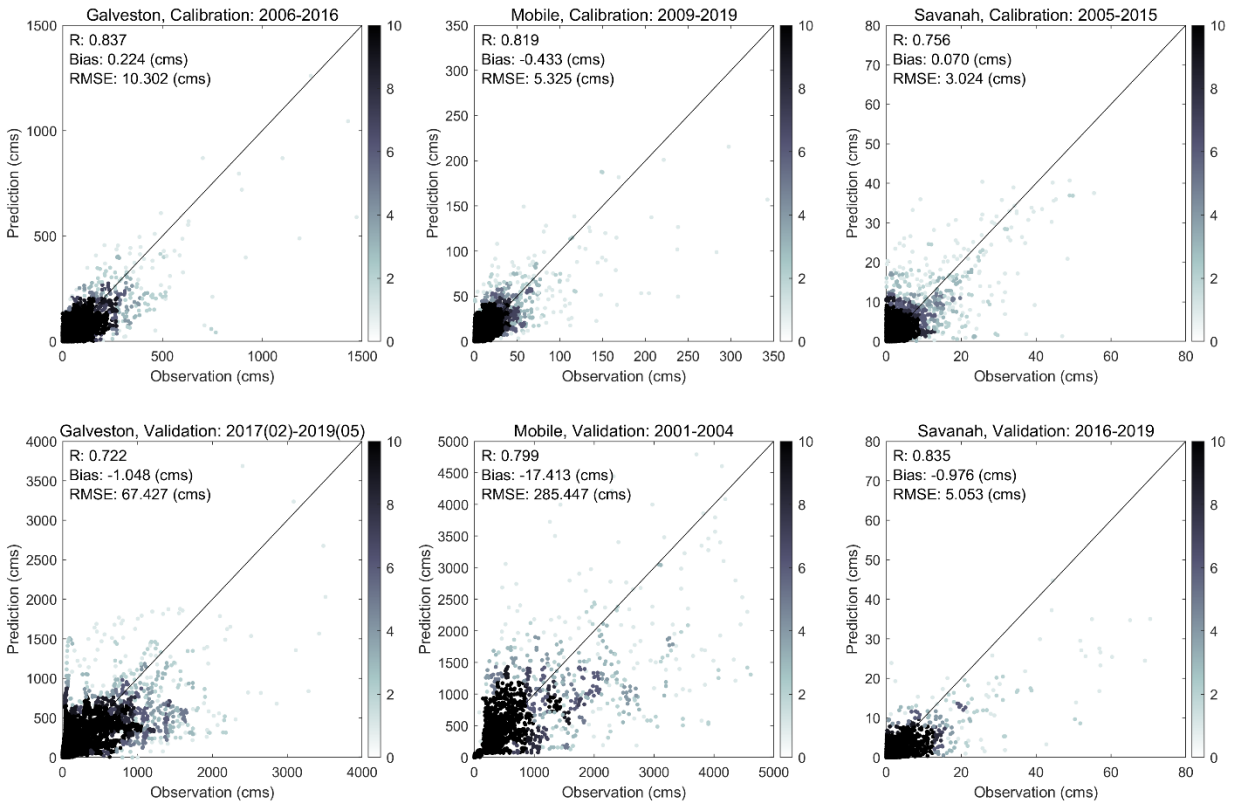

Figure 4. The performance of the SAC-SMA model during the calibration and validation periods over three watersheds in the southeast US.

Figure 5 illustrates the model performance (i.e., correlation coefficient and RMSE) across the USGS stations within the Galveston watershed. Figure S1 in the supplementary file shows the same results for the other two watersheds, Mobile and Savanah. The results for the Galveston watershed show that the calibrated SAC-SMA model accurately simulates the streamflow across almost the entire region except the two USGS stations located downstream of the Lake Livingston Dam. The primary function of this dam is flood control. Further analysis revealed that the lower performance of the model at these locations is attributed to the heavy rainfall of Hurricane Harvey that forced the Trinity River authority to release a record 110,600 ft^3/s from Lake Livingston Dam (The Seattle Times, 2021), which resulted in significantly increasing the river flow. A similar event happened in the case of Hurricane Rita that led to the significant flow increase in the Trinity River

and severe flooding (TPWD, 2021). Although the SAC-SMA hydrologic model successfully simulated river flow across all the USGS stations within the Galveston watershed, it could not provide reliable streamflow simulation along the Trinity River due to the water release from Lake Livingston Dam during the Hurricanes Rita and Harvey. For the Mobile watershed, as shown in Figure S1 in the supplementary file, there is a good agreement between the simulated and observed river discharge values across all USGS stations except station #02428400. Further investigations revealed that the river discharge at this location is computed based on flow through the Claiborne Dam (for more information, please see USGS, 2021b). During Hurricane Ivan, the flow at this USGS station reached more than 2800 m^3/s probably due to water release from the Claiborne Dam that consequently resulted in higher downstream river discharge.

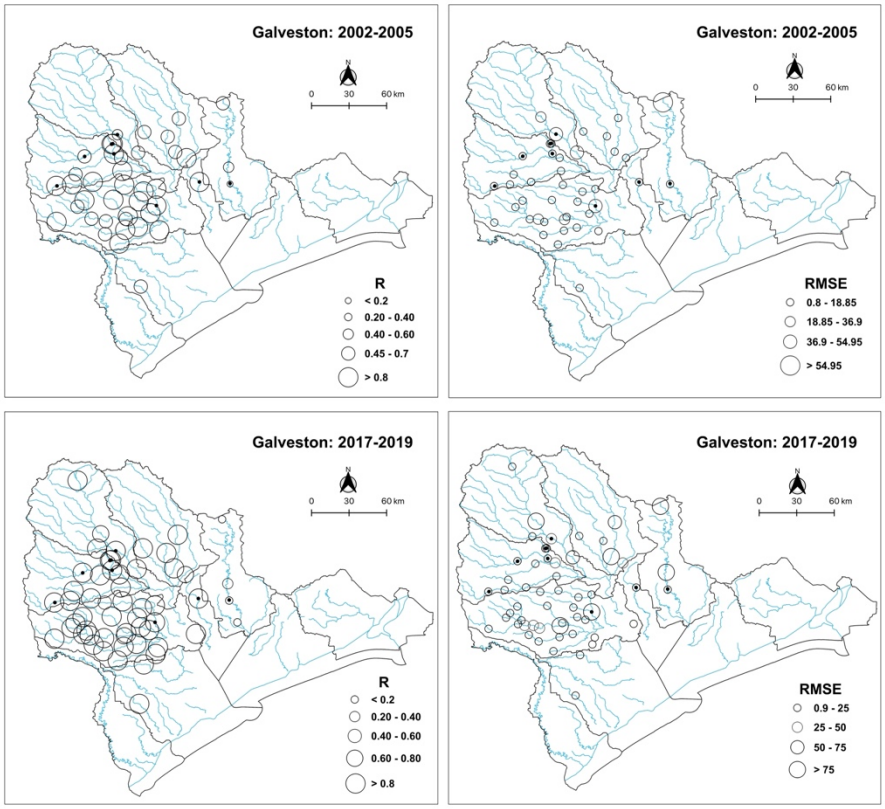

Figure 5. SAC-SMA model performance over the validation period across the USGS stations within the Galveston watershed. RMSE unit is m^3/s.

The NSE values for the calibration period were 0.80, 0.78, and 0.69 for Galveston, Mobile, and Savannah, respectively. Similarly, for the validation period, the NSE values for these regions were 0.68, 0.71, and 0.65, respectively. Figure 6 also illustrates the NSE for the USGS stations across the Galveston and Mobile watersheds. In this figure, positive NSE values are shown with black circles, and negative NSE values are shown with red circles. The regulated USGS stations are marked with black dots to facilitate interpretation of model performance at those specific locations. The results indicate that, in general, the model performance is lower at the regulated USGS stations. For example, the NSE for USGS station 8074000 (Figure 6) is negative; this station is located downstream of Addicks and Barker Dams.

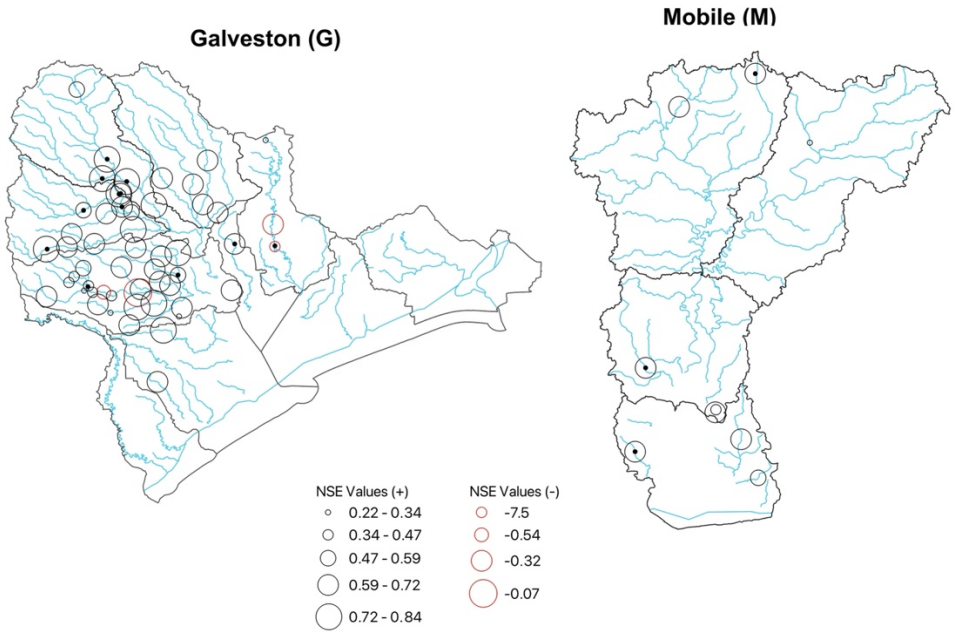

Figure 6. NSE values for the USGS stations across the Galveston and Mobile watersheds. This result is based on the validation period.

3.2 Improving Streamflow Forecasting using Data Assimilation

The primary goal of this research is to employ a data assimilation technique to account for all sources of uncertainty in SAC-SMA model simulation and provide a more accurate and reliable streamflow prediction. The data assimilation approach used in this study was developed recently by the authors of this study and is used here for the first time to predict streamflow values during multiple hurricane events with heavy rainfall across different locations in the SEUS. As previously stated, the primary objective of our study is to assess the degree to which the developed data assimilation technique improves the prediction of extreme river flow caused by hurricanes. This section summarizes the performance of the SAC-SMA model after using the data assimilation. The meteorological forcing data including precipitation and PET are assumed to have log-normal and normal error distributions with a relative error of 25% in the DA setting (DeChant and Moradkhani, 2012). This assumption ensures that the meteorological observations' errors due to spatial heterogeneity inherent in these variables and sensor errors are accounted for. The model error is assumed to follow a normal distribution with a relative error of 25%. Unlike the other data assimilation techniques, HEAVEN enables characterizing, quantifying, and taking into account the model structural uncertainty using an explicit form of model error covariance matrix within the data assimilation process. This feature of our developed data assimilation method is specifically more important in this study as we simulate the peak streamflow during hurricane events. As we discussed in our previous paper (Abbaszadeh et al., 2019), in this data assimilation technique, the background error covariance matrix B gets adaptively inflated when the model attempts to simulate extreme values. This error covariance matrix inflation not only helps the 4DVAR objective function to find the optimal initial condition within the assimilation window (Cheng et al., 2019; Liu et al., 2008; Trémolet, 2007), but also ensures exploring the larger feasible

494 solution space when the model states are being corrected within the particle filtering process,
495 which results in a more complete representation of posterior distributions. In summary, the
496 capability of the developed hydrologic data assimilation method to estimate peak flows stems from
497 its automatic process of inflating and deflating the background error covariance matrix. This
498 process enables the model to achieve a more realistic ensemble spread, leading to a more accurate
499 expected value compared to the observed value.

500 Here, we report the performance measures (i.e., correlation coefficient and RMSE) based
501 on an ensemble size of 100 for one-day ahead streamflow forecasting. Figures S2 and S3 show the
502 model performance after using data assimilation across all USGS stations located within the study
503 regions. It should be noted that these results are based on an ensemble size of 100, but of course,
504 larger ensemble sizes would have resulted in better posterior estimates and more accurate and
505 reliable streamflow forecasts. We realized that while data assimilation improved the SAC-SMA
506 model performance across the majority of stations, in some locations the results remained
507 suboptimal. Further investigation revealed that these are the same locations previously identified
508 as being heavily influenced by upstream dam water release during hurricane events. These
509 locations can not be used as upstream boundary conditions for hydrodynamic modeling (which is
510 part of our future study) as they are heavily influenced by water release policy during the hurricane
511 events that altered the natural flow of the river, where hydrologic models most often fail to
512 perform. Figure 7 depicts how data assimilation improved streamflow forecasting during peak
513 flow conditions across USGS stations in the Galveston watershed during Hurricane Harvey. Figure
514 7 shows the results for other watersheds and hurricane events, including Galveston-Rita, Mobile-
515 Ivan, Savanah-Matthew, and Savanah-Irma. In Figure 7, POI represents the percentage of
516 improvement achieved by performing the assimilation. In other words, it shows how much the

streamflow forecast improved (in percentage) by using data assimilation compared to the open-loop model simulation (without assimilation). The findings revealed that, while data assimilation improved the SAC-SMA streamflow forecasting skill almost across the entire USGS station networks on the peak flow day of Hurricane Harvey, its contribution to improving streamflow forecasting in Hurricane Rita is marginal. Unlike Hurricane Harvey where streamflow reached a peak gradually over the course of a few days (USGS, 2021a), in the case of Hurricane Rita, the streamflow jumped from less than 28 m^3/s (September 23) to more than 566 m^3/s (September 24) in a single day (according to station # 08066500 Trinity Rv at Romayor, TX), such that the hydrologic model failed to detect the unexpected high flow on September 24 despite accurate initialization on September 23 (USGS, 2021b).

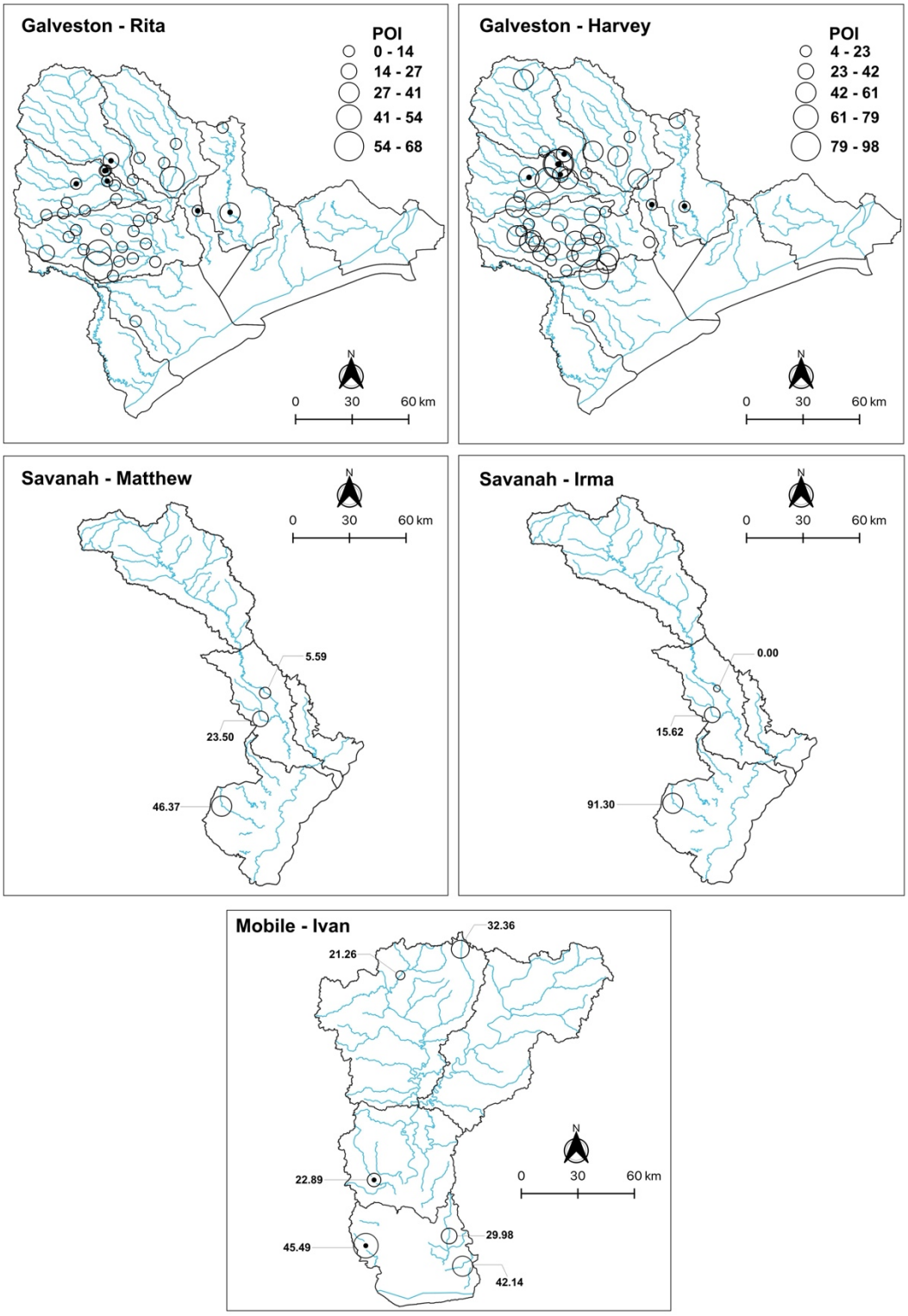

Figure 7. Streamflow forecast improved by data assimilation during peak flow conditions across the USGS stations within all three watersheds. The values shown for Savanah and Mobile stations are POI.

For Hurricanes Ivan and Matthew in Mobile and Savanah, the percentage of improvement in SAC-SMA model peak flow forecasts with data assimilation ranged from 21% to 46% and 5% to 46%, respectively, depending on the location of USGS stations. Understanding and explicitly quantifying the degree to which each source of uncertainties, i.e., meteorological forcing, model parameters, initial condition, model structure, and parametrization, affects the final hydrologic model outputs is not feasible as they all are connected and collectively contribute to degrading model performance. Our developed data assimilation technique, HEAVEN, has an explicit form of covariance error matrix for each source of uncertainty that feeds each other during the assimilation process representing the interaction between different sources of uncertainties involved in different layers of model simulations. This results in a better representation of posterior distribution and reduction of uncertainty in hydrologic modeling. Due to this reason, we see that the data assimilation approach used in this study is an effective technique to improve the streamflow forecasting skill during hurricane events.

Figure 8 illustrates the ensemble streamflow forecasts with and without using data assimilation across multiple USGS stations in the Galveston watershed. As it is seen in this figure, in all locations the ensemble mean is much closer to the observation compared to the streamflow mean value from the open-loop stimulation. The shaded blue area represents the 95% uncertainty interval. We also see that in all cases the observations fall within the uncertainty interval. Therefore, we can conclude that using data assimilation, the hydrologic model results in a more accurate and precise streamflow forecasts. In Figure 8, the green band represents the time window that contains the peak flow value, not just the peak itself. This band is intended to show the broader period during which the peak flow occurs, rather than the single peak value. The verification

process (POI reported in Figure 7) was based on this entire time window, including the period before and after the peak.

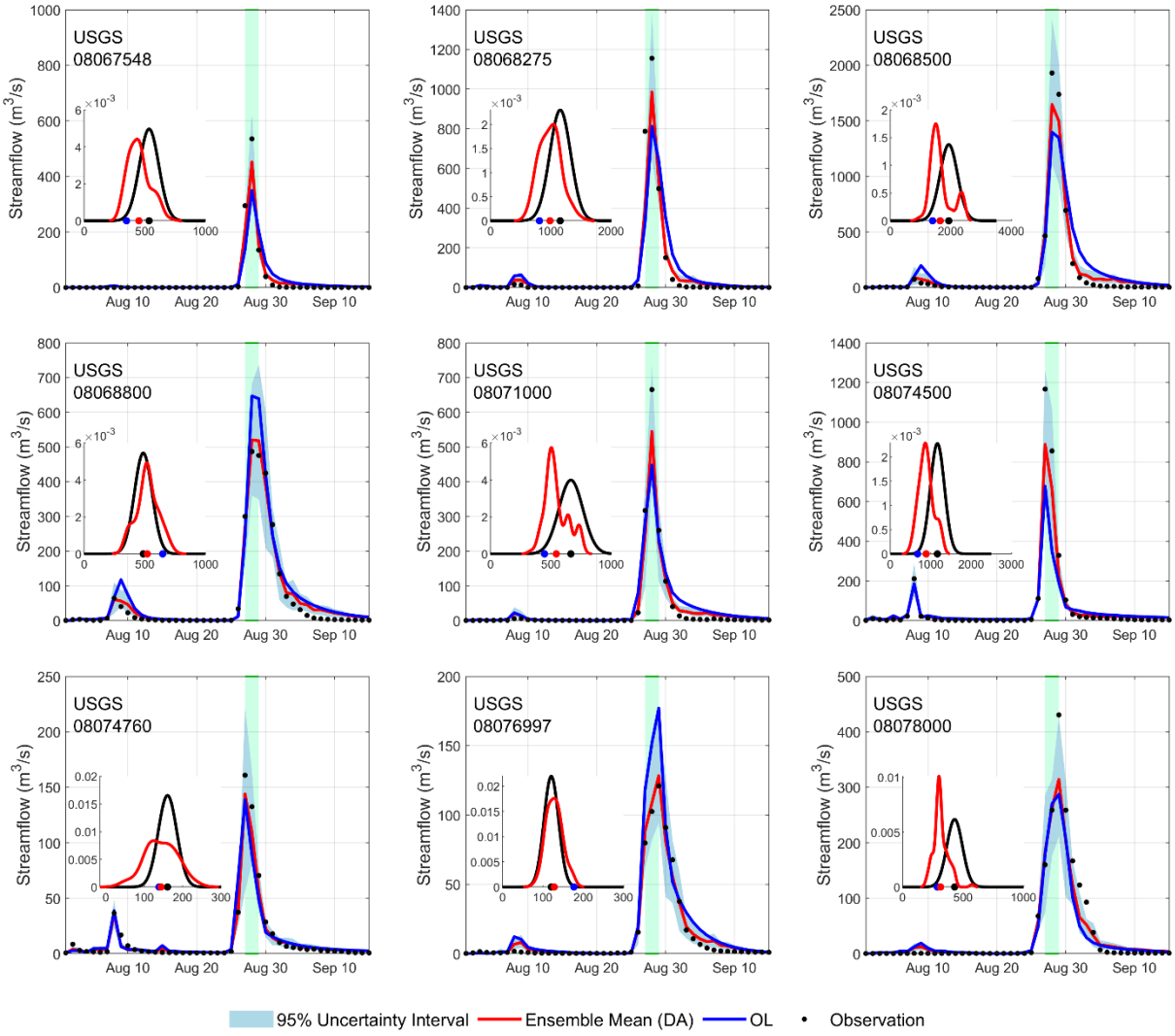

Figure 8. One-day ahead streamflow forecast with and without data assimilation across multiple USGS stations in the Galveston watershed in TX during Hurricane Harvey. The green band represents the time window that contains the peak flow value.

4. Conclusions

This study investigates the application of the HEAVEN data assimilation technique to improve the forecasting of extreme river flow during hurricane-induced flooding in the SEUS. By

564 integrating HEAVEN with the SAC-SMA hydrologic model, this research aimed to address the
565 various sources of uncertainty in hydrologic simulations, particularly during extreme events such
566 as hurricanes. The results show that HEAVEN effectively enhances the SAC-SMA model's
567 streamflow forecasting capabilities by incorporating uncertainty from multiple sources, including
568 meteorological forcing, model parameters, and structural errors.

569 The key findings highlight that data assimilation through HEAVEN significantly improved
570 streamflow forecasts during peak flow conditions, especially in cases where extreme river
571 discharge occurred. For example, in the Galveston watershed during Hurricane Harvey, data
572 assimilation led to substantial improvements in the forecasting of peak flows, with forecasted
573 values much closer to observed streamflow than those from the open-loop (non-assimilated)
574 model. However, in cases like Hurricane Rita, where the streamflow increased abruptly within a
575 very short time window, the assimilation approach was less effective. Despite accurate initial
576 conditions, the model struggled to capture the rapid onset of extreme flow, highlighting a limitation
577 of the current approach. This was due to the inability of the model to anticipate such a drastic shift
578 in flow within a single day, an event that may require further refinement of the assimilation process
579 to account for sudden, large fluctuations in discharge.

580 The HEAVEN technique proved capable of addressing model structural uncertainties by
581 inflating and deflating the background error covariance matrix, ensuring a more reliable posterior
582 distribution of streamflow forecasts. The assimilation process also facilitated the quantification
583 and interaction of multiple sources of uncertainty, improving the overall robustness of the
584 predictions. While the model performed well across most stations, some locations remained
585 challenging, particularly those influenced by water releases from upstream dams. These locations,

which significantly alter the natural flow dynamics, may require more specialized modeling approaches in future work, such as hydrodynamic modeling.

This study also discusses the computational limitations associated with optimizing the 4DVAR cost function using the Nelder-Mead algorithm, as the tangent linear or adjoint models were not available. While this approach is effective, it remains computationally intensive. With the growing use of Machine Learning (ML) emulators in hydrologic modeling, future work may focus on incorporating these techniques to accelerate optimization and further enhance the efficiency of data assimilation in large-scale hydrologic forecasting.

In summary, the HEAVEN data assimilation method offers a promising advancement in the accurate prediction of extreme river flow during hurricane events, but challenges remain in addressing sudden and large fluctuations in streamflow. Future developments may focus on refining the assimilation process for such events and incorporating additional modeling techniques, such as hydrodynamic models for regulated river systems, to further improve forecasting accuracy and reliability.

Appendix A: EPFM

EPFM is a sequential data assimilation technique based on the combination of particle filtering, Markov chain Monte Carlo (MCMC), and Genetic Algorithm (GA). EPFM is performed within the assimilation window for which the initial condition was obtained from the 4DVAR approach. Here we provide a brief overview of the EPFM algorithm and for more information, we refer the readers to the original article (Abbaszadeh et al., 2018). Equations A1 and A2 describe the generic nonlinear dynamic system, where $x_t \in \mathbb{R}^n$ and $\theta \in \mathbb{R}^d$ are vectors of uncertain state variables and model parameters, respectively. u_t represents the uncertain forcing data, $y_t \in$

$\mathbb{R}^m$ indicates a vector of observation data, ω_t and υ_t are the model and measurement errors, respectively, which are assumed to be independent and follow white noises with mean zero and covariance Q_t and R_t.

$$x_t = \mathcal{M}(x_{t-1}, u_t, \theta) + \omega_t \qquad \omega_t \sim N(0, Q_t) \qquad (A1)$$

$$y_t = h(x_t) + \upsilon_t \qquad \upsilon_t \sim N(0, R_t) \qquad (A2)$$

The following formula is used to calculate the posterior distribution of the state variables at time t.

$$p(x_t|y_{1:t}) = p(x_t|y_{1:t-1}, y_t) = \frac{p(y_t|x_t)p(x_t|y_{1:t-1})}{p(y_t|y_{1:t-1})} = \frac{p(y_t|x_t)p(x_t|y_{1:t-1})}{\int p(y_t|x_t)p(x_t|y_{1:t-1})dx_t} \qquad (A3)$$

$$p(x_t|y_{1:t-1}) = \int p(x_t, x_{t-1}|y_{1:t-1})dx_{t-1} = \int p(x_t|x_{t-1})p(x_{t-1}|y_{1:t-1})dx_{t-1} \qquad (A4)$$

where $p(y_t|x_t)$ is the likelihood at time step t, $p(x_t|y_{1:t-1})$ is the prior distribution, and $p(y_t|y_{1:t-1})$ is the normalization factor. The marginal likelihood function $p(y_{1:t})$ and the normalization factor $p(y_t|y_{1:t-1})$ can be calculated using equations A5 and A6, respectively.

$$p(y_{1:t}) = p(y_1)\prod\prod p(y_t|y_{1:t-1}) \qquad (A5)$$

$$p(y_t|y_{1:t-1}) = \int p(y_t, x_t|y_{1:t-1})dx_t = \int p(y_t|x_t)p(x_t|y_{1:t-1})dx_t \qquad (A6)$$

In hydrologic data assimilation using particle filtering, the posterior distribution is approximated by a set of particles, each with an associated weight.

$$p(x_t|y_{1:t}) \approx \sum_{i=1}^{N} w^{i+}\delta\left(x_t - x_t^i\right) \qquad (A7)$$

where w^{i+}, δ and N denote the posterior weight of the i-th particle, the Dirac delta function, and the ensemble size, respectively. The posterior weight is then normalized as follows:

$$w^{i+} = \frac{w^{i-}.\, p\left(y_t \middle| x_t^i, \theta_t^i\right)}{\sum_{i=1}^{N} w^{i-}.\, p\left(y_t \middle| x_t^i, \theta_t^i\right)} \qquad (A8)$$

where w^{i-} is the prior particle weights, and the $p\left(y_t \middle| x_t^i, \theta_t^i\right)$ can be computed from the likelihood $L\left(y_t \middle| x_t^i, \theta_t^i\right)$. To calculate this, for simplicity, a Gaussian likelihood is used as follows:

$$L\left(y_t \middle| x_t^i, \theta_t^i\right) = \frac{1}{\sqrt{(2\pi)^m |R_t|}} \exp\left[-\frac{1}{2}\left(y_t - h\left(x_t^i\right)\right)^T {R_t}^{-1} \left(y_t - h\left(x_t^i\right)\right)\right] \qquad (A9)$$

In this data assimilation method, a GA evolutionary cycle is employed to shuffle the particles. The weights of the particles (w^{i+}) are treated as their fitness values. The particles (or population) are sorted in descending order of fitness, and the roulette wheel selection method is applied to choose parent particles for the crossover operation, generating offspring (new particles). The crossover probability determines the proportion of particles involved in the crossover process. To enhance the diversity of the offspring, a mutation operator is applied with a specified probability. For further details on the crossover and mutation operators and their respective equations, we refer readers to Abbaszadeh et al. (2018). Finally, the MCMC approach is used to either accept or reject the newly generated offspring particles (proposed state variables). This process requires re-running the model from $t-1$ to t using x_{t-1}^i (state variables before using GA operators) and $x_{t-1}^{i,p}$ (state variables after using GA operators). To accept or reject the proposal states, the metropolis acceptance ratio α is calculated using equation A10.

$$\alpha = \min\left(1, \frac{p\left(x_t^{i,p}, \theta_t^{i-} \middle| y_{1:t}\right)}{p\left(x_t^{i-}, \theta_t^{i-} \middle| y_{1:t}\right)}\right) = \min\left(1, \frac{p\left(y_{1:t} \middle| x_t^{i,p}, \theta_t^{i-}\right).\, p\left(x_t^{i,p} \middle| \theta_t^{i-}, y_{1:t-1}\right)}{p\left(y_{1:t} \middle| x_t^{i-}, \theta_t^{i-}\right).\, p\left(x_t^{i-} \middle| \theta_t^{i-}, y_{1:t-1}\right)}\right) \qquad (A10)$$

where $p\left(x_t^{i,p}, \theta_t^{i-} \middle| y_{1:t}\right)$ is the proposed joint probability distribution.

$$p\left(x_t^{i,p}, \theta_t^{i-} \middle| y_{1:t}\right) \propto p\left(y_t \middle| x_t^{i,p}, \theta_t^{i-}\right). p\left(x_t^{i,p} \middle| \theta_t^{i-}, y_{1:t-1}\right). p\left(\theta_t^{i-} \middle| y_{1:t-1}\right) \qquad (A11)$$

$$x_t^{i,p} = \mathcal{M}\left(x_{t-1}^{i,p}, u_t^i, \theta_t^{i-}\right) \qquad (A12)$$

where $p\left(y_t \middle| x_t^{i,p}, \theta_t^{i-}\right)$ is computed using equation A9 and the proposal state Probability Density Function (PDF) $p\left(x_t^{i,p} \middle| \theta_t^{i-}, y_{1:t-1}\right)$ is calculated with the assumption that it follows the marginal Gaussian distributions with mean μ_t (Eq. A14) and variance σ_t^2 (Eq. A15). To calculate the proposal PDF, the weighted mean and variance of the Gaussian distribution are calculated as follows:

$$x_t^{i-} = \mathcal{M}\left(x_{t-1}^{i+}, u_t^i, \theta_t^{i-}\right) \qquad (A13)$$

$$\mu_t = \sum w_{t-1}^{i+} x_t^{i-} \qquad (A14)$$

$$\sigma_t^2 = \sum w_{t-1}^{i+} \left(x_t^{i-} - \mu_t\right)^2 \qquad (A15)$$

Using the accepted proposal state variables, the posterior weights are recalculated using equation A8, and these weights are then used to compute the effective sample size. The resampling step in the sequential data assimilation approach has been detailed in our previous work (Moradkhani et al., 2012), and we refer readers to that publication for further information.

Appendix B: How Is Variational Data Assimilation Coupled with Sequential Data Assimilation?

The Hybrid Ensemble and Variational Data Assimilation Framework for Environmental Systems method combines EPFM with 4DVAR data assimilation. Its goal is to robustly estimate

model states and parameters while accounting for structural, parameter, and input uncertainties in environmental systems. The hybrid framework leverages the sequential updating capability of EPFM and the batch optimization strengths of 4DVAR to address uncertainties at various stages of the modeling process. In this paper, we focus on how the prior (background) error covariance matrix B is updated during the sequential filtering process. This matrix is then used in the next assimilation cycle within the 4DVAR cost function. By applying equation A16, we obtain the best estimates of the model state variables and parameters as the expected values of their posterior distributions at each time step within the assimilation window.

$$\bar{x}_k^+ = \frac{1}{N}\sum_{i=1}^{N} x_k^{i+} \quad \text{and} \quad \bar{\theta}_k^+ = \frac{1}{N}\sum_{i=1}^{N} \theta_k^{i+} \qquad \forall k = 1, \ldots, K \tag{A16}$$

$$\eta_k = \bar{x}_k^+ - \mathcal{M}_{k-1\to k}(\bar{x}_{k-1}^+, \bar{\theta}_k^+, u_k) \tag{A17}$$

$$q = \frac{1}{K}\sum_{k=1}^{K} \eta_k \tag{A18}$$

$$B_d = \frac{1}{K-1}\sum_{k=1}^{K} [\eta_k - q][\eta_k - q]^T \tag{A19}$$

$$B_s = B \tag{A20}$$

$$B = (\gamma \times B_s) + (1-\gamma) \times B_d \qquad 0 \le \gamma \le 1 \tag{A21}$$

η_k and q represent the estimate of model error and model error bias at each time within the assimilation window. In this approach, the EPFM filter is applied within the assimilation window, where the best initial condition is estimated using the 4DVAR method. A key challenge arises in how to use the deterministic (single) initial condition obtained from 4DVAR to initialize the EPFM filter, which is an ensemble-based approach. To address this, we define a prior error covariance matrix B, consisting of two components: dynamic (B_d) and static (B_s) prior error covariances, to

perturb the deterministic solution from the 4DVAR method and generate the best initial condition for the EPFM filter. The dynamic prior error covariance matrix B_d is introduced by Shaw and Daescu (2016) in the assimilation cycle, while B represents the prior error covariance matrix from the previous assimilation cycle. The static prior error covariance matrix B_s is used in the current assimilation cycle. The prior error covariance matrix B is updated using equation A21. The tuning factor γ controls the contribution of model error within the current assimilation cycle.

Appendix C: The Implementation Process

1. Initialization

Three essential error covariance matrices are initialized. This section highlights how different sources of uncertainties are accounted for with the proposed approach.

- **Prior Error Covariance (B)**: Combines dynamic (B_d) and static (B_s) components:

  $$\mathbf{B} = (\gamma \times B_s) + (1 - \gamma) \times B_d \qquad 0 \leq \gamma \leq 1 \qquad (A21)$$

- **Observation Error Covariance ($\mathbf{R_k}$)**: Assumes observation errors are Gaussian:

  $$\mathbf{R_k} = (\max((\lambda \times y_k), 1))^2 \qquad \text{Eq. 2 (section 2.4)}$$

  where λ is the observation error percentage.

- **Model Error Covariance ($\mathbf{Q_k}$):** initialized as:

  $$Q_k = \Gamma \times \mathrm{diag}\left((\pi \times x_{0,b})^2\right) \qquad \text{Eq. 4 (section 2.4)}$$

  where π is the error percentage in model structure, and Γ is an inflation or deflation factor.

- Parameters (Θ) and initial ensembles (x_0^i) are generated using Latin Hypercube Sampling (LHS).

2. Variational Initialization (Step 1)

A deterministic state estimation is performed using 4DVAR. This step minimizes the cost function that combines prior, observational, and model error contributions. To avoid the need for model

linearization, derivative-free optimization methods like the Nelder-Mead algorithm are used to find optimal solutions. The 4DVAR method minimizes a cost function to estimate the optimal state x_a for the assimilation window $[t_0, t_k]$. The cost function incorporates prior, observation, and model error terms:

- $\mathrm{J}(\mathrm{x}_0, \ldots, \mathrm{x}_\mathrm{K}) = \mathrm{J}^\mathrm{b} + \mathrm{J}^\mathrm{o} + \mathrm{J}^\mathrm{q}$

where

Background Term ($\mathbf{J^b}$): This term penalizes deviations of the initial state x_0 from the background (or prior) state $x_{0,b}$. It is weighted by the inverse of the prior error covariance matrix B.

- $\mathrm{J}^\mathrm{b} = \frac{1}{2}\left(\mathrm{x}_0 - \mathrm{x}_{0,\mathrm{b}}\right)^\mathrm{T} \mathrm{B}^{-1}\left(\mathrm{x}_0 - \mathrm{x}_{0,\mathrm{b}}\right)$

Observation Term ($\mathbf{J^o}$): This term penalizes the difference between the model-predicted observations $h(x_k)$ and the actual observations y_k over all time steps within the assimilation window.

- $\frac{1}{2}\sum_{\mathrm{k}=0}^{\mathrm{K}}\left(\mathrm{y}_\mathrm{k} - \mathrm{h}_\mathrm{k}(\mathrm{x}_\mathrm{k})\right)^\mathrm{T} \mathrm{R}_\mathrm{k}^{-1}\left(\mathrm{y}_\mathrm{k} - \mathrm{h}_\mathrm{k}(\mathrm{x}_\mathrm{k})\right)$

Model Error Term ($\mathbf{J^q}$): This term accounts for discrepancies between the model-predicted state at time k and the actual state x_k. It reflects the uncertainty in the model dynamics.

- $\frac{1}{2}\sum_{\mathrm{k}=1}^{\mathrm{K}}(\mathrm{x}_\mathrm{k} - \mathcal{M}_{\mathrm{k}-1\to\mathrm{k}}(\mathrm{x}_{\mathrm{k}-1}, \Theta, \mathrm{u}_\mathrm{k}))^\mathrm{T}\, \mathrm{Q}^{-1}(\mathrm{x}_\mathrm{k} - \mathcal{M}_{\mathrm{k}-1\to\mathrm{k}}(\mathrm{x}_{\mathrm{k}-1}, \Theta, \mathrm{u}_\mathrm{k}))$

$h(x_k)$: Observation operator at time k.

$M_{\mathrm{k}-1\to\mathrm{k}}$: Model transition operator between $k-1$ and k.

To avoid linearization of M and h, derivative-free optimization methods (e.g., Nelder-Mead) are employed.

3. Ensemble Generation (Step 2)

The deterministic 4DVAR solution is perturbed using the prior error covariance matrix B, resulting in an initial ensemble of states for particle filtering. This step bridges the sequential and variational components. The deterministic 4DVAR solution x_a is perturbed using the prior error covariance matrix B to generate an ensemble:

- $x_0^i = x_a + \varepsilon^i \qquad \varepsilon^i \sim N(0, B)$ Eq. 6 (section 2.4)

4. Sequential Assimilation via EPFM (Step 3)

The EPFM filter updates states and parameters sequentially by approximating the posterior distribution $p(x_t|y_{1:t})$.

- $p(x_t|y_{1:t}) \propto p(y_t|x_t)p(x_t|y_{1:t-1})$

$p(y_t|x_t)$: Prior distribution

$(x_t|y_{1:t-1})$: Likelihood of observations.

The posterior is represented as a weighted ensemble:

- $p(x_t|y_{1:t}) \approx \sum_{i=1}^{N} w^{i+}\delta(x_t - x_t^i)$ Eq. A7 (Appendix A)

To avoid particle degeneracy, an evolutionary Monte Carlo approach combines GA with MCMC. The mutation and crossover steps in GA ensure particle diversity, while MCMC refines the posterior ensemble. See (Appendix A) for more information.

5. Updating Error Covariance Matrices (Step 4-5)

The dynamic error covariance matrix B_d is estimated using ensemble-based error propagation:

- $\eta_k = \bar{x}_k^+ - \mathcal{M}_{k-1\to k}(\bar{x}_{k-1}^+, \bar{\theta}_k^+, u_k)$ Eq. A17 (Appendix A)
- $q = \frac{1}{K}\sum_{k=1}^{K}\eta_k$ Eq. A18 (Appendix A)
- $B_d = \frac{1}{K-1}\sum_{k=1}^{K}[\eta_k - q][\eta_k - q]^T$ Eq. A19 (Appendix A)

The prior error covariance B is updated as:

- $B = (\gamma \times B_s) + (1 - \gamma) \times B_d$ Eq. A21 (Appendix A)

6. Iterative Feedback Loop

The updated BB and EPFM posterior states feed back into the 4DVAR method as prior conditions for the next assimilation cycle. This iterative exchange ensures consistent improvement of states and parameters over time.

Appendix D: Uncertainty Handling in HEAVEN

HEAVEN explicitly handles uncertainties at multiple stages: *Model Structural Uncertainty*: Incorporated through dynamic error covariance B_d and feedback loops. *Parameter and Forcing Uncertainty*: Addressed via the EPFM ensemble framework. *Observation Uncertainty*: Modeled through R_k and integrated into the cost function. By combining sequential and variational approaches, HEAVEN offers a comprehensive solution for state and parameter estimation in nonlinear, uncertain systems. Steps where major uncertainties are addressed include: Generating the initial ensemble (Step 2). Dynamically updating B (Step 5) and using ensemble posterior information in feedback loops (Step 6).

Competing interests

The contact author has declared that none of the authors has any competing interests.

Acknowledgment

The partial financial support for this project was provided by the USACE -ERDC contract number A20-0545-001.

Authors Contributions

P.A. wrote the first draft of the manuscript, conducted all model simulations, and analyzed the results. F.G. assisted with the visualization of the results and providing the revised version of this manuscript. K.G. contributed to the collection and processing of remote sensing data. P.A. and H.M. conceptualized the study, and H.M. edited the manuscript.

References

Abbaszadeh, P., Gavahi, K., Moradkhani, H., 2020. Multivariate remotely sensed and in-situ data assimilation for enhancing community WRF-Hydro model forecasting. Adv. Water Resour. 145, 103721. https://doi.org/10.1016/j.advwatres.2020.103721

Abbaszadeh, P., Moradkhani, H., Daescu, D.N., 2019. The Quest for Model Uncertainty Quantification: A Hybrid Ensemble and Variational Data Assimilation Framework. Water Resour. Res. 55, 2407–2431. https://doi.org/10.1029/2018WR023629

Abbaszadeh, P., Moradkhani, H., Yan, H., 2018. Enhancing hydrologic data assimilation by evolutionary Particle Filter and Markov Chain Monte Carlo. Adv. Water Resour. 111, 192–204. https://doi.org/10.1016/j.advwatres.2017.11.011

Ahmadisharaf, E., Kalyanapu, A.J., Bates, P.D., 2018. A probabilistic framework for floodplain mapping using hydrological modeling and unsteady hydraulic modeling. Hydrol. Sci. J. 63. https://doi.org/10.1080/02626667.2018.1525615

Alipour, A., Ahmadalipour, A., Abbaszadeh, P., Moradkhani, H., 2020a. Leveraging machine learning for predicting flash flood damage in the Southeast US. Environ. Res. Lett. 15, 024011. https://doi.org/10.1088/1748-9326/ab6edd

Alipour, A., Ahmadalipour, A., Moradkhani, H., 2020b. Assessing flash flood hazard and damages in the southeast United States. J. Flood Risk Manag. 13. https://doi.org/10.1111/jfr3.12605

Anderson, J.L., Anderson, S.L., 1999. A Monte Carlo Implementation of the Nonlinear Filtering Problem to Produce Ensemble Assimilations and Forecasts. Mon. Weather Rev. 127, 2741–2758. https://doi.org/10.1175/1520-0493(1999)127<2741:AMCIOT>2.0.CO;2

Annis, A., Nardi, F., Volpi, E., Fiori, A., 2020. Quantifying the relative impact of hydrological and hydraulic modelling parameterizations on uncertainty of inundation maps. Hydrol. Sci. J. 65. https://doi.org/10.1080/02626667.2019.1709640

Apel, H., Thieken, A.H., Merz, B., Blöschl, G., 2004. Flood risk assessment and associated uncertainty. Nat. Hazards Earth Syst. Sci. 4. https://doi.org/10.5194/nhess-4-295-2004

Aronica, G., Bates, P.D., Horritt, M.S., 2002. Assessing the uncertainty in distributed model predictions using observed binary pattern information within GLUE. Hydrol. Process. 16. https://doi.org/10.1002/hyp.398

Bateni, S.M., Entekhabi, D., 2012. Surface heat flux estimation with the ensemble Kalman smoother: Joint estimation of state and parameters. Water Resour. Res. 48, 1–16. https://doi.org/10.1029/2011WR011542

Bates, P.D., Horritt, M.S., Aronica, G., Beven, K., 2004. Bayesian updating of flood inundation likelihoods conditioned on flood extent data. Hydrol. Process. 18. https://doi.org/10.1002/hyp.1499

Bennett, K.E., Cherry, J.E., Balk, B., Lindsey, S., 2019. Using MODIS estimates of fractional snow cover area to improve streamflow forecasts in interior Alaska. Hydrol. Earth Syst. Sci. 23. https://doi.org/10.5194/hess-23-2439-2019

Bermúdez, M., Neal, J.C., Bates, P.D., Coxon, G., Freer, J.E., Cea, L., Puertas, J., 2017. Quantifying local rainfall dynamics and uncertain boundary conditions into a nested regional-local flood modeling system. Water Resour. Res. 53. https://doi.org/10.1002/2016WR019903

Bhuyian, M.N.M., Kalyanapu, A.J., Nardi, F., 2015. Approach to Digital Elevation Model Correction by Improving Channel Conveyance. J. Hydrol. Eng. 20. https://doi.org/10.1061/(asce)he.1943-5584.0001020

Blöschl, G., Hall, J., Viglione, A., Perdigão, R.A.P., Parajka, J., Merz, B., Lun, D., Arheimer, B., Aronica, G.T., Bilibashi, A., Boháč, M., Bonacci, O., Borga, M., Čanjevac, I., Castellarin, A., Chirico, G.B., Claps, P., Frolova, N., Ganora, D., Gorbachova, L., Gül, A., Hannaford, J., Harrigan, S., Kireeva, M., Kiss, A., Kjeldsen, T.R., Kohnová, S., Koskela, J.J., Ledvinka, O., Macdonald, N., Mavrova-Guirguinova, M., Mediero, L., Merz, R., Molnar, P., Montanari, A., Murphy, C., Osuch, M., Ovcharuk, V., Radevski, I., Salinas, J.L., Sauquet, E., Šraj, M., Szolgay, J., Volpi, E., Wilson, D., Zaimi, K., Živković, N., 2019. Changing climate both increases and decreases European river floods. Nature 573. https://doi.org/10.1038/s41586-019-1495-6

Bowman, A.L., Franz, K.J., Hogue, T.S., 2017. Case studies of a MODIS-based potential evapotranspiration input to the Sacramento Soil Moisture Accounting model. J. Hydrometeorol. 18. https://doi.org/10.1175/JHM-D-16-0214.1

Bravo, J.M., Allasia, D., Paz, A.R., Collischonn, W., Tucci, C.E.M., 2012. Coupled Hydrologic-Hydraulic Modeling of the Upper Paraguay River Basin. J. Hydrol. Eng. 17. https://doi.org/10.1061/(asce)he.1943-5584.0000494

Burnash, R., Ferral, R., Richard A. McGuire, 1973. A generalized streamflow simulation system, NOAA Technical Report.

Cheng, S., Argaud, J.-P., Iooss, B., Lucor, D., Ponçot, A., 2019. Background error covariance iterative updating with invariant observation measures for data assimilation. Stoch. Environ. Res. Risk Assess. 33, 2033–2051. https://doi.org/10.1007/s00477-019-01743-6

Clark, M.P., Rupp, D.E., Woods, R.A., Zheng, X., Ibbitt, R.P., Slater, A.G., Schmidt, J., Uddstrom, M.J., 2008a. Hydrological data assimilation with the ensemble Kalman filter: Use of streamflow observations to update states in a distributed hydrological model. Adv. Water Resour. 31, 1309–1324. https://doi.org/10.1016/j.advwatres.2008.06.005

Clark, M.P., Rupp, D.E., Woods, R.A., Zheng, X., Ibbitt, R.P., Slater, A.G., Schmidt, J., Uddstrom, M.J., 2008b. Hydrological data assimilation with the ensemble Kalman filter: Use of streamflow observations to update states in a distributed hydrological model. Adv. Water Resour. 31, 1309–1324. https://doi.org/10.1016/j.advwatres.2008.06.005

Dechant, C.M., Moradkhani, H., 2012. Examining the effectiveness and robustness of sequential data assimilation methods for quantification of uncertainty in hydrologic forecasting. Water Resour. Res. 48, 1–15. https://doi.org/10.1029/2011WR011011

Dechant, C.M., Moradkhani, H., 2011. Improving the characterization of initial condition for ensemble streamflow prediction using data assimilation. Hydrol. Earth Syst. Sci. 15, 3399–3410. https://doi.org/10.5194/hess-15-3399-2011

DeChant, C.M., Moradkhani, H., 2012. Examining the effectiveness and robustness of sequential data assimilation methods for quantification of uncertainty in hydrologic forecasting. Water Resour. Res. 48. https://doi.org/10.1029/2011WR011011

Di Baldassarre, G., Montanari, A., 2009. Uncertainty in river discharge observations: A quantitative analysis. Hydrol. Earth Syst. Sci. 13. https://doi.org/10.5194/hess-13-913-2009

Dimitriadis, P., Tegos, A., Oikonomou, A., Pagana, V., Koukouvinos, A., Mamassis, N., Koutsoyiannis, D., Efstratiadis, A., 2016. Comparative evaluation of 1D and quasi-2D hydraulic models based on benchmark and real-world applications for uncertainty assessment in flood mapping. J. Hydrol. 534. https://doi.org/10.1016/j.jhydrol.2016.01.020

Domeneghetti, A., Castellarin, A., Brath, A., 2012. Assessing rating-curve uncertainty and its effects on hydraulic model calibration. Hydrol. Earth Syst. Sci. 16. https://doi.org/10.5194/hess-16-1191-2012

Domeneghetti, A., Vorogushyn, S., Castellarin, A., Merz, B., Brath, A., 2013. Probabilistic flood hazard mapping: Effects of uncertain boundary conditions. Hydrol. Earth Syst. Sci. 17. https://doi.org/10.5194/hess-17-3127-2013

Duan, Q., Sorooshian, S., Gupta, V., 1992. Effective and efficient global optimization for conceptual rainfall-runoff models. Water Resour. Res. 28, 1015–1031. https://doi.org/10.1029/91WR02985

Duan, Q.Y., Gupta, V.K., Sorooshian, S., 1993. Shuffled complex evolution approach for effective and efficient global minimization. J. Optim. Theory Appl. 76. https://doi.org/10.1007/BF00939380

Earth Data Science, 2021. Acquiring streamflow data from USGS with climata and Python [WWW Document]. URL https://www.earthdatascience.org/tutorials/acquire-and-visualize-usgs-hydrology-data/ (accessed 11.11.21).

Felder, G., Zischg, A., Weingartner, R., 2017. The effect of coupling hydrologic and hydrodynamic models on probable maximum flood estimation. J. Hydrol. 550. https://doi.org/10.1016/j.jhydrol.2017.04.052

Grimaldi, S., Petroselli, A., Arcangeletti, E., Nardi, F., 2013. Flood mapping in ungauged basins using fully continuous hydrologic-hydraulic modeling. J. Hydrol. 487. https://doi.org/10.1016/j.jhydrol.2013.02.023

888 Grimaldi, S., Schumann, G.J.P., Shokri, A., Walker, J.P., Pauwels, V.R.N., 2019. Challenges,
889 Opportunities, and Pitfalls for Global Coupled Hydrologic-Hydraulic Modeling of Floods.
890 Water Resour. Res. 55. https://doi.org/10.1029/2018WR024289

891 Gourley, J. J., Flamig, Z. L., Hong, Y., & Howard, K. W. 2014. Evaluation of past, present and
892 future tools for radar-based flash-flood prediction in the USA. Hydrological Sciences
893 Journal, 59(7), 1377–1389. https://doi.org/10.1080/02626667.2014.919391

894 Hain, C.R., Crow, W.T., Anderson, M.C., Mecikalski, J.R., 2012. An ensemble Kalman filter
895 dual assimilation of thermal infrared and microwave satellite observations of soil moisture
896 into the Noah land surface model. Water Resour. Res. 48.
897 https://doi.org/10.1029/2011WR011268

898 Ingram, K., Dow, K., Carter, L. Anderson, J. (Eds.): Climate in the Southeastern United States:
899 Variability, Change, Impacts and Vulnerability, Island Press, Washington DC, 2013.

900 Jafarzadegan, K., H. Moradkhani, F. Pappenberger, H. Moftakhari, P. Bates, P. Abbaszadeh, R.
901 Marsooli, C. Ferreira, H. Cloke, F. Ogden, and D. Qingyun (2023), Recent Advances and
902 New Frontiers in Riverine and Coastal Flood Modeling, Reviews of Geophysics,
903 doi:10.1007/s11625-023-01298-0

904 John P. Cangialosi, Andrew S. Latto, and R.B., 2017. NATIONAL HURRICANE CENTER
905 TROPICAL CYCLONE REPORT: HURRICANE IRMA.

906 Kratzert, F., Klotz, D., Brenner, C., Schulz, K., Herrnegger, M. 2018. Rainfall–runoff modelling
907 using Long Short-Term Memory (LSTM) networks. Hydrol. Earth Syst. Sci. 22, 6005–
908 6022. https://doi.org/10.5194/hess-22-6005-2018.

909 Koster, R.D., Liu, Q., Mahanama, S.P.P., Reichle, R.H., 2018. Improved Hydrological
910 Simulation Using SMAP Data: Relative Impacts of Model Calibration and Data
911 Assimilation. J. Hydrometeorol. 19, 727–741. https://doi.org/10.1175/JHM-D-17-0228.1

912 Knox, P., & Mogil, M. 2020. The weather and climate of Georgia: Georgia's "peachy" weather
913 and climate: Something for everyone. Weatherwise, 73(5), 40–41.
914 https://doi.org/10.1080/00431672.2020.1787719

915 Kuczera, G., Parent, E., 1998. Monte Carlo assessment of parameter uncertainty in conceptual
916 catchment models: the Metropolis algorithm. J. Hydrol. 211, 69–85.
917 https://doi.org/10.1016/S0022-1694(98)00198-X

918 Laganier, O., Ayral, P.A., Salze, D., Sauvagnargues, S., 2014. A coupling of hydrologic and
919 hydraulic models appropriate for the fast floods of the Gardon River basin (France). Nat.
920 Hazards Earth Syst. Sci. 14. https://doi.org/10.5194/nhess-14-2899-2014

921 Lee, H.;,Seo, D.-J., Noh, S.J. 2016. A weakly-constrained data assimilation approach to address
922 rainfall-runoff model structural inadequacy in streamflow prediction. J. Hydrol. 542, 373–
923 391.

924 Lee, H., Seo, D.J., Koren, V., 2011. Assimilation of streamflow and in situ soil moisture data
925 into operational distributed hydrologic models: Effects of uncertainties in the data and
926 initial model soil moisture states. Adv. Water Resour. 34, 1597–1615.
927 https://doi.org/10.1016/j.advwatres.2011.08.012

928 Lian, Y., Chan, I.C., Singh, J., Demissie, M., Knapp, V., Xie, H., 2007. Coupling of hydrologic
929 and hydraulic models for the Illinois River Basin. J. Hydrol. 344.
930 https://doi.org/10.1016/j.jhydrol.2007.08.004

931 Liberto, T. Di, 2016. Record-breaking hurricane Matthew causes devastation [WWW
932 Document]. NOAA Clim. URL https://www.climate.gov/news-features/event-
933 tracker/record-breaking-hurricane-matthew-causes-devastation

934 Lievens, H., De Lannoy, G.J.M., Al Bitar, A., Drusch, M., Dumedah, G., Hendricks Franssen,
935 H.J., Kerr, Y.H., Tomer, S.K., Martens, B., Merlin, O., Pan, M., Roundy, J.K., Vereecken,
936 H., Walker, J.P., Wood, E.F., Verhoest, N.E.C., Pauwels, V.R.N., 2016. Assimilation of
937 SMOS soil moisture and brightness temperature products into a land surface model. Remote
938 Sens. Environ. 180, 292–304. https://doi.org/10.1016/j.rse.2015.10.033

939 Liu, C., Xiao, Q., Wang, B., 2008. An ensemble-based four-dimensional variational data
940 assimilation scheme. Part I: Technical formulation and preliminary test. Mon. Weather Rev.
941 136. https://doi.org/10.1175/2008MWR2312.1

942 Liu, Y., Gupta, H. V., 2007. Uncertainty in hydrologic modeling: Toward an integrated data
943 assimilation framework. Water Resour. Res. https://doi.org/10.1029/2006WR005756

944 Liu, Z., Merwade, V., Jafarzadegan, K., 2019. Investigating the role of model structure and
945 surface roughness in generating flood inundation extents using one- and two-dimensional
946 hydraulic models. J. Flood Risk Manag. 12. https://doi.org/10.1111/jfr3.12347

947 Mai, D.T., De Smedt, F., 2017. A combined hydrological and hydraulic model for flood
948 prediction in Vietnam applied to the Huong river basin as a test case study. Water
949 (Switzerland) 9. https://doi.org/10.3390/w9110879

950 Mallakpour, I., Villarini, G., 2015. The changing nature of flooding across the central United
951 States. Nat. Clim. Chang. 5. https://doi.org/10.1038/nclimate2516

952 Marshall, L., Nott, D., Sharma, A., 2004. A comparative study of Markov chain Monte Carlo
953 methods for conceptual rainfall-runoff modeling. Water Resour. Res. 40, 1–11.
954 https://doi.org/10.1029/2003WR002378

955 Montanari, M., Hostache, R., Matgen, P., Schumann, G., Pfister, L., Hoffmann, L., 2009.
956 Calibration and sequential updating of a coupled hydrologic-hydraulic model using remote
957 sensing-derived water stages. Hydrol. Earth Syst. Sci. 13. https://doi.org/10.5194/hess-13-
958 367-2009

959 Montzka, C., Grant, J.P., Moradkhani, H., Franssen, H.-J.H., Weihermüller, L., Drusch, M.,
960 Vereecken, H., 2013. Estimation of Radiative Transfer Parameters from L-Band Passive
961 Microwave Brightness Temperatures Using Advanced Data Assimilation. Vadose Zo. J. 12.
962 https://doi.org/10.2136/vzj2012.0040

963 Moradkhani, H., DeChant, C.M., Sorooshian, S., 2012. Evolution of ensemble data assimilation
964 for uncertainty quantification using the particle filter-Markov chain Monte Carlo method.
965 Water Resour. Res. 48. https://doi.org/10.1029/2012WR012144

966 Moradkhani, H., Hsu, K.-L., Gupta, H., Sorooshian, S., 2005. Uncertainty assessment of
967 hydrologic model states and parameters: Sequential data assimilation using the particle

968 filter. Water Resour. Res. 41, 1–17. https://doi.org/10.1029/2004WR003604

969 Moradkhani, H., Nearing, G., Abbaszadeh, P., Pathiraja, S., 2018a. Fundamentals of Data
970 Assimilation and Theoretical Advances, in: Handbook of Hydrometeorological Ensemble
971 Forecasting. Springer Berlin Heidelberg, pp. 1–26. https://doi.org/10.1007/978-3-642-
972 40457-3_30-1

973 Moradkhani, H., Nearing, G., Abbaszadeh, P., Pathiraja, S., 2018b. Fundamentals of Data
974 Assimilation and Theoretical Advances. Handb. Hydrometeorol. Ensemble Forecast. 1–26.
975 https://doi.org/10.1007/978-3-642-40457-3_30-1

976 Mu, Q., Heinsch, F.A., Zhao, M., Running, S.W., 2007. Development of a global
977 evapotranspiration algorithm based on MODIS and global meteorology data. Remote Sens.
978 Environ. 111. https://doi.org/10.1016/j.rse.2007.04.015

979 Mu, Q., Zhao, M., Running, S.W., 2011. Improvements to a MODIS global terrestrial
980 evapotranspiration algorithm. Remote Sens. Environ. 115.
981 https://doi.org/10.1016/j.rse.2011.02.019

982 Nam, D.H., Mai, D.T., Udo, K., Mano, A., 2014. Short-term flood inundation prediction using
983 hydrologic-hydraulic models forced with downscaled rainfall from global NWP. Hydrol.
984 Process. 28. https://doi.org/10.1002/hyp.10084

985 Neal, J.C., Odoni, N.A., Trigg, M.A., Freer, J.E., Garcia-Pintado, J., Mason, D.C., Wood, M.,
986 Bates, P.D., 2015. Efficient incorporation of channel cross-section geometry uncertainty
987 into regional and global scale flood inundation models. J. Hydrol. 529.
988 https://doi.org/10.1016/j.jhydrol.2015.07.026

989 Nelder, J.A., Mead, R., 1965. A Simplex Method for Function Minimization. Comput. J. 7, 308–
990 313. https://doi.org/10.1093/comjnl/7.4.308

991 Nguyen, P., Thorstensen, A., Sorooshian, S., Hsu, K., AghaKouchak, A., Sanders, B., Koren, V.,
992 Cui, Z., Smith, M., 2016. A high resolution coupled hydrologic–hydraulic model
993 (HiResFlood-UCI) for flash flood modeling. J. Hydrol. 541.
994 https://doi.org/10.1016/j.jhydrol.2015.10.047

995 NOAA, 2005. Hurricane Ivan Tropical Cyclone Report. National Hurricane Center.
996 https://www.nhc.noaa.gov/data/tcr/AL092004_Ivan.pdf

997 Papaioannou, G., Vasiliades, L., Loukas, A., Aronica, G.T., 2017. Probabilistic flood inundation
998 mapping at ungauged streams due to roughness coefficient uncertainty in hydraulic
999 modelling. Adv. Geosci. 44. https://doi.org/10.5194/adgeo-44-23-2017

1000 Pappenberger, F., Beven, K., Horritt, M., Blazkova, S., 2005. Uncertainty in the calibration of
1001 effective roughness parameters in HEC-RAS using inundation and downstream level
1002 observations. J. Hydrol. 302. https://doi.org/10.1016/j.jhydrol.2004.06.036

1003 Pappenberger, F., Matgen, P., Beven, K.J., Henry, J.B., Pfister, L., Fraipont, P., 2006. Influence
1004 of uncertain boundary conditions and model structure on flood inundation predictions. Adv.
1005 Water Resour. 29. https://doi.org/10.1016/j.advwatres.2005.11.012

1006 Pathiraja, S., Anghileri, D., Burlando, P., Sharma, A., Marshall, L., Moradkhani, H., 2018a.

Insights on the impact of systematic model errors on data assimilation performance in changing catchments. Adv. Water Resour. 113, 202–222. https://doi.org/S030917081730670X

Pathiraja, S., Moradkhani, H., Marshall, L., Sharma, A., Geenens, G., 2018b. Data-Driven Model Uncertainty Estimation in Hydrologic Data Assimilation. Water Resour. Res. https://doi.org/10.1002/2018WR022627

Petroselli, A., Vojtek, M., Vojteková, J., 2019. Flood mapping in small ungauged basins: A comparison of different approaches for two case studies in Slovakia. Hydrol. Res. 50. https://doi.org/10.2166/nh.2018.040

Plaza, D.A., De Keyser, R., De Lannoy, G.J.M., Giustarini, L., Matgen, P., Pauwels, V.R.N., 2012. The importance of parameter resampling for soil moisture data assimilation into hydrologic models using the particle filter. Hydrol. Earth Syst. Sci. 16, 375–390. https://doi.org/10.5194/hess-16-375-2012

Richard D. Knabb, Daniel P. Brown, and J.R.R., 2006. Tropical Cyclone Report Hurricane Rita.

Ryan McNeill and Duff Wilson, 2017. Exclusive: At least $23 billion of property affected by Hurricane Harvey - Reuters analysis [WWW Document]. Reuters. URL https://www.reuters.com/article/us-storm-harvey-property-exclusive/exclusive-at-least-23-billion-of-property-affected-by-hurricane-harvey-reuters-analysis-idUSKCN1BA31P

Samuel, J., Coulibaly, P., Metcalfe, R.A., 2011. Estimation of Continuous Streamflow in Ontario Ungauged Basins: Comparison of Regionalization Methods. J. Hydrol. Eng. 16. https://doi.org/10.1061/(asce)he.1943-5584.0000338

Savant, G., Berger, C., McAlpin, T.O., Tate, J.N., 2011. Efficient Implicit Finite-Element Hydrodynamic Model for Dam and Levee Breach. J. Hydraul. Eng. 137. https://doi.org/10.1061/(asce)hy.1943-7900.0000372

Savant, G., Berger, R.C., 2012. Adaptive Time Stepping–Operator Splitting Strategy to Couple Implicit Numerical Hydrodynamic and Water Quality Codes. J. Environ. Eng. 138. https://doi.org/10.1061/(asce)ee.1943-7870.0000547

Scharffenberg, W.A., Kavvas, M.L., 2011. Uncertainty in Flood Wave Routing in a Lateral-Inflow-Dominated Stream. J. Hydrol. Eng. 16. https://doi.org/10.1061/(asce)he.1943-5584.0000298

Shaw, J.A., Daescu, D.N., 2016. An ensemble approach to weak-constraint four-dimensional variational data assimilation. Procedia Comput. Sci. 80, 496–506. https://doi.org/10.1016/j.procs.2016.05.329

Sindhu, K., Durga Rao, K.H.V., 2017. Hydrological and hydrodynamic modeling for flood damage mitigation in Brahmani–Baitarani River Basin, India. Geocarto Int. 32. https://doi.org/10.1080/10106049.2016.1178818

Smith, M.B., Laurine, D.P., Koren, V.I., Reed, S.M., Zhang, Z., 2003. Hydrologic Model calibration in the National Weather Service. pp. 133–152. https://doi.org/10.1029/WS006p0133

Stewart, S.R., 2017. National Hurricane Center Tropical Cyclone Report: Hurricane Matthew. Natl. Hurric. Cent. Trop. Cyclone Rep. 5.

The Seattle Times, 2021. Harvey recovery continues in parts of flooded Liberty County [WWW Document]. URL https://www.seattletimes.com/nation-world/harvey-recovery-continues-in-parts-of-flooded-liberty-county/ (accessed 11.11.21).

Thomas Steven Savage, J., Pianosi, F., Bates, P., Freer, J., Wagener, T., 2016. Quantifying the importance of spatial resolution and other factors through global sensitivity analysis of a flood inundation model. Water Resour. Res. 52. https://doi.org/10.1002/2015WR018198

TPWD [WWW Document], 2021. URL https://tpwd.texas.gov/newsmedia/releases/?req=20050927a (accessed 11.11.21).

Tripathy, S., K. Jafarzadegan, H. Moftakhari, and H. Moradkhani (2024), Dynamic Bivariate Hazard Forecasting of Hurricanes for Improved Disaster Preparedness, Communications Earth & Environment, doi:10.1038/s43247-023-01198-2

Trémolet, Y., 2007. Model-error estimation in 4D-Var. Q. J. R. Meteorol. Soc. 133, 1267–1280. https://doi.org/10.1002/qj.94

USGS, 2021a. USGS [WWW Document]. URL https://waterdata.usgs.gov/nwis/dv/?ts_id=133980,173616,173617&format=img_default&site_no=08066500&begin_date=20170817&end_date=20170906 (accessed 11.11.21).

USGS, 2021b. USGS [WWW Document]. URL https://waterdata.usgs.gov/nwis/dv/?ts_id=133980,173616,173617&format=img_default&site_no=08066500&begin_date=20050918&end_date=20050930 (accessed 11.11.21).

USGS [WWW Document], 2021c. URL https://waterdata.usgs.gov/usa/nwis/uv?site_no=02428400 (accessed 11.11.21).

Vacondio, R., Dal Palù, A., Mignosa, P., 2014. GPU-enhanced finite volume shallow water solver for fast flood simulations. Environ. Model. Softw. 57. https://doi.org/10.1016/j.envsoft.2014.02.003

Vrugt, J.A., Gupta, H. V., Nualláin, B.Ó., Bouten, W., 2006. Real-time data assimilation for operational ensemble streamflow forecasting. J. Hydrometeorol. 7, 548–565. https://doi.org/10.1175/JHM504.1

Wahlstrom, M., Guha-Sapir, D., 2015. The human cost of weather-related disasters 1995-2015, UNISDR Publications.

Werner, M., Blazkova, S., Petr, J., 2005. Spatially distributed observations in constraining inundation modelling uncertainties. Hydrol. Process. 19. https://doi.org/10.1002/hyp.5833

Xia, Y., Mitchell, K., Ek, M., Sheffield, J., Cosgrove, B., Wood, E., Luo, L., Alonge, C., Wei, H., Meng, J., Livneh, B., Lettenmaier, D., Koren, V., Duan, Q., Mo, K., Fan, Y., Mocko, D., 2012. Continental-scale water and energy flux analysis and validation for the North American Land Data Assimilation System project phase 2 (NLDAS-2): 1. Intercomparison and application of model products. J. Geophys. Res. 117, 1–27. https://doi.org/10.1029/2011JD016048

Yan, H., DeChant, C.M., Moradkhani, H., 2015. Improving Soil Moisture Profile Prediction With the Particle Filter-Markov Chain Monte Carlo Method. IEEE Trans. Geosci. Remote Sens. 53, 6134–6147. https://doi.org/10.1109/TGRS.2015.2432067

Yan, H., Moradkhani, H., 2016. Combined assimilation of streamflow and satellite soil moisture with the particle filter and geostatistical modeling. Adv. Water Resour. 94, 364–378. https://doi.org/10.1016/j.advwatres.2016.06.002

Zischg, A.P., Felder, G., Mosimann, M., Röthlisberger, V., Weingartner, R., 2018. Extending coupled hydrological-hydraulic model chains with a surrogate model for the estimation of flood losses. Environ. Model. Softw. 108. https://doi.org/10.1016/j.envsoft.2018.08.009